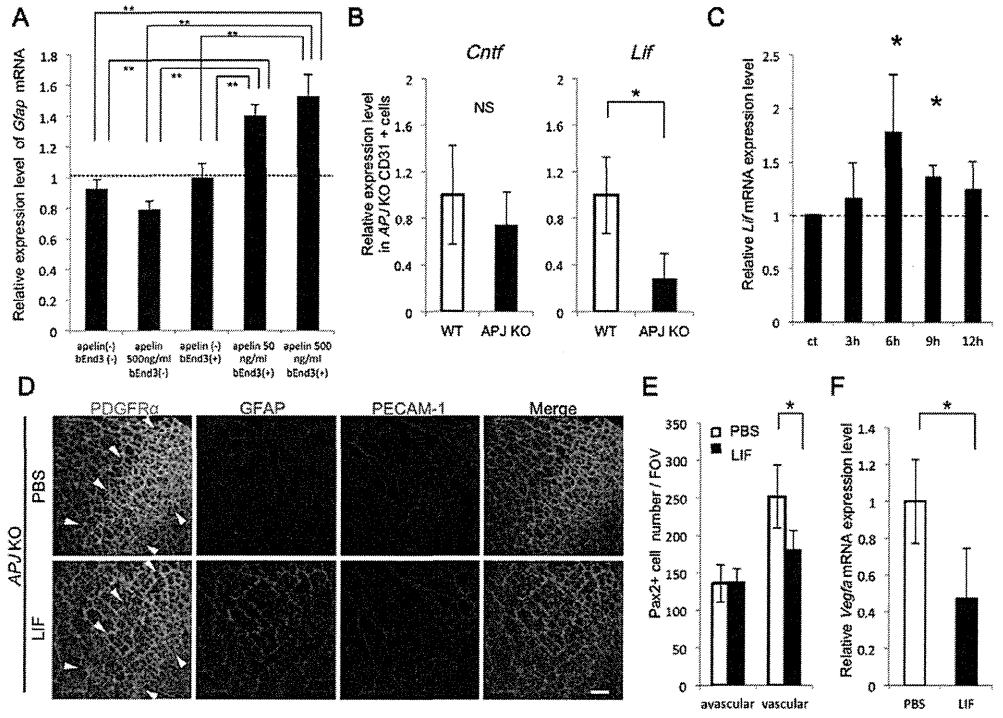


**Fig. 7. Overgrowth of immature astrocytes resulting from the lack of APJ in ECs is prevented by LIF.** (**A**) Effect on astrocyte GFAP positivity of medium conditioned by bEnd3 ECs stimulated with 50 ng/ml or 500 ng/ml apelin. Total RNA was extracted from dissociated retinal cells 24 hours after treatment with conditioned medium and qPCR analysis was performed to examine the expression of *Gfap* mRNA. $^{**}P<0.01$. (**B**) qPCR analysis of *Cntf* and *Lif* using RNA isolated from FACS-sorted PECAM1$^+$ ECs of P6 mouse retinas ($n=4$, $^*P<0.05$; N.S., not significant). (**C**) qPCR analysis of *LIF* mRNA expression in HUVECs. Total RNA was extracted from HUVECs stimulated with 50 ng/ml apelin for 0-12 hours ($n=3$, $^*P<0.05$). (**D-F**) Effects of LIF on aberrant outgrowth of ECs and astrocytes. (D) Retinas of P5 *APJ* KO mice were dissected 48 hours after intraocular injection of PBS or LIF and stained with antibodies against PDGFRα, GFAP and PECAM1. LIF inhibited astrocyte proliferation (surrounded by arrowheads) and induced upregulation of GFAP even ahead of the sprouting edge. Scale bar: 100 μm. (E) Quantitative evaluation of the number of PAX2$^+$ astrocytes in vascular or avascular areas of *APJ* KO retina after treatment with PBS or LIF ($n=3$, $^*P<0.05$). (F) qPCR analysis of *Vegfa* mRNA expression in sorted PDGFRα$^+$ cells of P5 PBS- or LIF-treated *APJ* KO retinas ($n=3$, $^*P<0.05$). Error bars indicate s.d.

acids. It is possible that apelin affects ECs that are continuously expressing APJ in the retina, not only locally but also in a wider context. While apelin in the retina has been reported to have proangiogenic properties (del Toro et al., 2010), we previously reported that it also acts as a maturation factor for newly developing blood vessels. It induces the assembly of ECs, and thus promotes the formation of larger blood vessels (Kidoya et al., 2008). It also stabilizes the junction protein VE-cadherin and thus inhibits vascular hyperpermeability induced by VEGF or inflammatory stimuli (Kidoya et al., 2010). Therefore, diverse functions for apelin during angiogenesis have been postulated. VEGF has strong proangiogenic activity, but also induces the production of vasohibin 1, which has anti-angiogenic activity (Watanabe et al., 2004). This implies that proangiogenic factors might also concurrently induce anti-angiogenic factors in ECs as part of a negative-feedback regulatory mechanism. LIF production from ECs upon activation of APJ might also be involved in such a negative-feedback system during angiogenesis. Based on the phenotype of *Apln* KO or *APJ* KO mice, we conclude that apelin facilitates angiogenesis by inducing proliferation of ECs, but subsequently indirectly finalizes angiogenesis by furthering the maturation of astrocytes in the retina. Therefore, delay of capillary outgrowth from the optic nerve head, and the suppression of vascular network formation, are primarily defects induced by the lack of APJ or apelin. The partial hypervascularity subsequently observed in the migrating front of the vascular network-forming area is, indirectly, a secondary deficit caused by insufficient maturation of astrocytes.

We previously reported that TIE2 activation by ANG1 in ECs is one pathway of apelin production (Kidoya et al., 2008). Consistent with ANG1 regulating the enlargement of blood vessels, we found that apelin also induces enlarged blood vessels by promoting the assembly of ECs. Based on these findings, we reported apelin as a factor for constructing enlarged blood vessels and that it acts as a downstream regulator of the ANG1/TIE2 system. We initially focused on enlargement of blood vessels in retinas from *APJ* KO mice. However, *APJ* KO mice showed moderate defects of vascular network formation in their retinas and we could not clearly compare vascular diameters because of delayed blood vessel formation in these mice.

ANG1 production is usually induced in mural cells, which are located beside both tip cells and stalk cells. With respect to mural cell localization, WT and *APJ* KO mice were indistinguishable (supplementary material Fig. S4). Therefore, ANG1 might affect both tip cells and stalk cells. Because apelin mRNA is expressed predominantly in tip cells in the retina (del Toro et al., 2010; Strasser et al., 2010), these might possess a specific machinery for apelin production, which could be affected by ANG1. However, mechanisms regulating apelin production in tip cells have not been elucidated. It has previously been reported that ANG1 is produced by astrocytes upon re-oxygenation after ischemia and has been suggested to play an important role in the barrier function associated with tight junction proteins (Lee et al., 2003). We previously reported that apelin also induces stabilization of VE-cadherin in ECs, as

described above (Kidoya et al., 2010). Therefore, further studies of the relationship between ANG1 and apelin and of the additional involvement of other mechanisms regulating apelin production in tip cells as influenced by mural cells or astrocytes are required.

In the brain, neural precursor cells (NPCs) generate neurons and subsequently glia. This switch is crucial for determination of the number of neurons and glia. Mechanisms regulating the differentiation of glia from NPCs, such as how and where the commitment to the glial lineage is made, have been extensively analyzed (Freeman, 2010; Rowitch and Kriegstein, 2010). However, regulation of astrocyte differentiation from immature to mature cells in vivo is not well characterized. One line of evidence suggests that oxygen levels control astrocyte differentiation, i.e. inadequate vascularity in the retina induces hypoxia, resulting in the suppression of astrocyte differentiation (West et al., 2005). Reciprocally, well-organized vascular formation triggers maturation of astrocytes under normoxia. Deficiency of APJ also induces hypoxia because of insufficient outgrowth of blood vessels; such hypoxia may then induce hypervascularity caused by VEGF upregulation and release from immature astrocytes. It is possible that maturation arrest of astrocytes might be secondary to the lack of APJ; however, we found that expression of LIF, an astrocyte maturation factor, is induced in ECs by stimulation with apelin. Because LIF expression is reduced in *APJ* KO mice, these data suggest that complex mechanisms, such as hypoxia and attenuation of LIF, underlie the suppression of astrocyte maturation in *APJ* KO mice.

Although it has been reported that LIF secreted by ECs induces astrocyte maturation (Kubota et al., 2008; Mi et al., 2001), how LIF is induced in ECs in vivo has not been determined. Our present data suggest that LIF production mediated by activation of APJ in ECs by apelin is one of the programmed processes regulating maturation of astrocytes in vivo, which facilitates well-organized vascular and astrocyte network formation in the retina. However, it has been reported that *Lif* KO mice show overall hypervascularity in their retinas (Kubota et al., 2008) and this phenotype is different from that of *APJ* KO mice because hypervascularity was restricted to the migrating front of the vascular network area in these latter mice. GFAP positivity in astrocytes at areas other than the migrating front of the vascular network did not differ between WT and *APJ* KO mice (Fig. 2A). This suggests the existence of mechanisms other than the apelin/APJ system for astrocyte maturation and indicates that further investigation is required to achieve a full understanding of the molecular mechanisms of blood vessel and astrocyte maturation.

**Acknowledgements**
Special thanks are due to Yoshiaki Kubota (Department of Cell Differentiation, Sakaguchi Laboratory, School of Medicine, Keio University, Shinjuku-ku, Tokyo, Japan) for outstanding technical support. We also thank Ping Xie for technical support and Keisho Fukuhara and Noriko Fujimoto for general assistance.

**Funding**
This work was partly supported by a grant from the Ministry of Education, Science, Sports, and Culture of Japan.

**Competing interests statement**
The authors declare no competing financial interests.

**Supplementary material**
Supplementary material available online at
http://dev.biologists.org/lookup/suppl/doi:10.1242/dev.072330/-/DC1

**References**

**Augustin, H. G., Koh, G. Y., Thurston, G. and Alitalo, K.** (2009). Control of vascular morphogenesis and homeostasis through the angiopoietin-Tie system. *Nat. Rev. Mol. Cell Biol.* **10**, 165-177.

**Bonni, A., Sun, Y., Nadal-Vicens, M., Bhatt, A., Frank, D. A., Rozovsky, I., Stahl, N., Yancopoulos, G. D. and Greenberg, M. E.** (1997). Regulation of gliogenesis in the central nervous system by the JAK-STAT signaling pathway. *Science* **278**, 477-483.

**Chu, Y., Hughes, S. and Chan-Ling, T.** (2001). Differentiation and migration of astrocyte precursor cells and astrocytes in human fetal retina: relevance to optic nerve coloboma. *FASEB J.* **15**, 2013-2015.

**del Toro, R., Prahst, C., Mathivet, T., Siegfried, G., Kaminker, J. S., Larrivee, B., Breant, C., Duarte, A., Takakura, N., Fukamizu, A. et al.** (2010). Identification and functional analysis of endothelial tip cell-enriched genes. *Blood* **116**, 4025-4033.

**Freeman, M. R.** (2010). Specification and morphogenesis of astrocytes. *Science* **330**, 774-778.

**Fruttiger, M., Calver, A. R., Kruger, W. H., Mudhar, H. S., Michalovich, D., Takakura, N., Nishikawa, S. and Richardson, W. D.** (1996). PDGF mediates a neuron-astrocyte interaction in the developing retina. *Neuron* **17**, 1117-1131.

**Gariano, R. F.** (2003). Cellular mechanisms in retinal vascular development. *Prog. Retin. Eye Res.* **22**, 295-306.

**Gerhardt, H., Golding, M., Fruttiger, M., Ruhrberg, C., Lundkvist, A., Abramsson, A., Jeltsch, M., Mitchell, C., Alitalo, K., Shima, D. et al.** (2003). VEGF guides angiogenic sprouting utilizing endothelial tip cell filopodia. *J. Cell Biol.* **161**, 1163-1177.

**Ishida, J., Hashimoto, T., Hashimoto, Y., Nishiwaki, S., Iguchi, T., Harada, S., Sugaya, T., Matsuzaki, H., Yamamoto, R., Shiota, N. et al.** (2004). Regulatory roles for APJ, a seven-transmembrane receptor related to angiotensin-type 1 receptor in blood pressure in vivo. *J. Biol. Chem.* **279**, 26274-26279.

**Kasai, A., Shintani, N., Kato, H., Matsuda, S., Gomi, F., Haba, R., Hashimoto, H., Kakuda, M., Tano, Y. and Baba, A.** (2008). Retardation of retinal vascular development in apelin-deficient mice. *Arterioscler. Thromb. Vasc. Biol.* **28**, 1717-1722.

**Kidoya, H., Ueno, M., Yamada, Y., Mochizuki, N., Nakata, M., Yano, T., Fujii, R. and Takakura, N.** (2008). Spatial and temporal role of the apelin/APJ system in the caliber size regulation of blood vessels during angiogenesis. *EMBO J.* **27**, 522-534.

**Kidoya, H., Naito, H. and Takakura, N.** (2010). Apelin induces enlarged and nonleaky blood vessels for functional recovery from ischemia. *Blood* **115**, 3166-3174.

**Kishimoto, T., Akira, S., Narazaki, M. and Taga, T.** (1995). Interleukin-6 family of cytokines and gp130. *Blood* **86**, 1243-1254.

**Kubota, Y., Hirashima, M., Kishi, K., Stewart, C. L. and Suda, T.** (2008). Leukemia inhibitory factor regulates microvessel density by modulating oxygen-dependent VEGF expression in mice. *J. Clin. Invest.* **118**, 2393-2403.

**Kurihara, T., Kubota, Y., Ozawa, Y., Takubo, K., Noda, K., Simon, M. C., Johnson, R. S., Suematsu, M., Tsubota, K., Ishida, S. et al.** (2010). von Hippel-Lindau protein regulates transition from the fetal to the adult circulatory system in retina. *Development* **137**, 1563-1571.

**Lee, S. W., Kim, W. J., Choi, Y. K., Song, H. S., Son, M. J., Gelman, I. H., Kim, Y. J. and Kim, K. W.** (2003). SSeCKS regulates angiogenesis and tight junction formation in blood-brain barrier. *Nat. Med.* **9**, 900-906.

**Mi, H., Haeberle, H. and Barres, B. A.** (2001). Induction of astrocyte differentiation by endothelial cells. *J. Neurosci.* **21**, 1538-1547.

**Rowitch, D. H. and Kriegstein, A. R.** (2010). Developmental genetics of vertebrate glial-cell specification. *Nature* **468**, 214-222.

**Saint-Geniez, M., Argence, C. B., Knibiehler, B. and Audigier, Y.** (2003). The msr/apj gene encoding the apelin receptor is an early and specific marker of the venous phenotype in the retinal vasculature. *Gene Expr. Patterns* **3**, 467-472.

**Sato, T. N., Tozawa, Y., Deutsch, U., Wolburg-Buchholz, K., Fujiwara, Y., Gendron-Maguire, M., Gridley, T., Wolburg, H., Risau, W. and Qin, Y.** (1995). Distinct roles of the receptor tyrosine kinases Tie-1 and Tie-2 in blood vessel formation. *Nature* **376**, 70-74.

**Strasser, G. A., Kaminker, J. S. and Tessier-Lavigne, M.** (2010). Microarray analysis of retinal endothelial tip cells identifies CXCR4 as a mediator of tip cell morphology and branching. *Blood* **115**, 5102-5110.

**Suri, C., Jones, P. F., Patan, S., Bartunkova, S., Maisonpierre, P. C., Davis, S., Sato, T. N. and Yancopoulos, G. D.** (1996). Requisite role of angiopoietin-1, a ligand for the TIE2 receptor, during embryonic angiogenesis. *Cell* **87**, 1171-1180.

**Takakura, N., Watanabe, T., Suenobu, S., Yamada, Y., Noda, T., Ito, Y., Satake, M. and Suda, T.** (2000). A role for hematopoietic stem cells in promoting angiogenesis. *Cell* **102**, 199-209.

**Uemura, A., Kusuhara, S., Wiegand, S. J., Yu, R. T. and Nishikawa, S.** (2006). Tlx acts as a proangiogenic switch by regulating extracellular assembly of fibronectin matrices in retinal astrocytes. *J. Clin. Invest.* **116**, 369-377.

**Watanabe, K., Hasegawa, Y., Yamashita, H., Shimizu, K., Ding, Y., Abe, M., Ohta, H., Imagawa, K., Hojo, K., Maki, H. et al.** (2004). Vasohibin as an endothelium-derived negative feedback regulator of angiogenesis. *J. Clin. Invest.* **114**, 898-907.

**West, H., Richardson, W. D. and Fruttiger, M.** (2005). Stabilization of the retinal vascular network by reciprocal feedback between blood vessels and astrocytes. *Development* **132**, 1855-1862.

**Zhang, Y. and Stone, J.** (1997). Role of astrocytes in the control of developing retinal vessels. *Invest. Ophthalmol. Vis. Sci.* **38**, 1653-1666.

Oncogene (2012) 31, 3254–3264

www.nature.com/onc

ORIGINAL ARTICLE

# The apelin/APJ system induces maturation of the tumor vasculature and improves the efficiency of immune therapy

H Kidoya[1,4], N Kunii[2,3,4], H Naito[1], F Muramatsu[1], Y Okamoto[2], T Nakayama[3] and N Takakura[1]

[1]*Department of Signal Transduction, Research Institute for Microbial Diseases, Osaka University, Osaka, Japan;* [2]*Department of Otorhinolaryngology and Head and Neck Surgery, Graduate School of Medicine, Chiba University, Chiba, Japan and* [3]*Department of Immunology, Graduate School of Medicine, Chiba University, Chiba, Japan*

**Immature and unstable tumor vasculature provides an aberrant tumor microenvironment and leads to resistance of tumors to conventional therapy. Hence, normalization of tumor vessels has been reported to improve the effect of immuno-, chemo- and radiation therapy. However, the humoral factors, which can effectively induce maturation of tumor vasculature, have not been elucidated. In this study, we found that the novel peptide apelin and its receptor APJ can induce the morphological and functional maturation of blood vessels in tumors. This apelin-induced tumor vascular maturation enhances the efficacy of cancer dendritic cell-based immunotherapy and significantly suppresses tumor growth by promoting the infiltration of invariant natural killer T cells into the central region of the tumor and thereby robustly inducing apoptosis of tumor cells. Additionally, we showed APJ expression to be enhanced in the tumor endothelium in comparison with normal-state endothelial cells. These findings provide a new target for tumor vascular-specific maturation, which is expected to improve the efficacy of conventional cancer therapies.**

*Oncogene* (2012) **31,** 3254–3264; doi:10.1038/onc.2011.489; published online 31 October 2011

**Keywords:** tumor angiogenesis; immune therapy; vascular normalization; vascular maturation; apelin/APJ

## Introduction

Agents targeting the tumor vasculature have been used for antitumor therapy in various preclinical and clinical studies (Gasparini *et al.*, 2005; Heath and Bicknell, 2009). The function of vascular endothelial growth factor (VEGF)-family ligands and their receptors in tumor angiogenesis has been well established, and serves as a logical target for antiangiogenic cancer therapy (Lohela *et al.*, 2009).The anti-VEGF monoclonal antibody, bevacizumab, neutralizes all isoforms of human VEGF (Gerber and Ferrara, 2005). Combining bevacizumab with chemotherapeutic agents appears to result in modest survival benefit in patients with metastatic colorectal cancer (Hurwitz *et al.*, 2004). This antitumor effect of bevacizumab was assumed to be due to its disruption of VEGF, and it was expected to directly suppress endothelial cell (EC) growth and inhibit tumor angiogenesis. However, Jain and co-workers recently showed that anti-angiogenic therapy causes 'normalization' of aberrant tumor vasculature and thus induces the formation of functional mature vasculature (Jain, 2005). This normalization of the tumor vasculature is effective for combination antitumor therapies, because mature vasculature and increased blood flow to tumors can promote the delivery of antitumor therapeutics to tumor cells (Dickson *et al.*, 2007). Therefore, investigating the role played by endogenous vascular maturation factors during the angiogenesis process could help in the development of a new antitumor therapy.

Apelin, a secreted peptide, has been identified as the endogenous ligand of the G-protein-coupled cell-surface receptor APJ (Tatemoto *et al.*, 1998). Apelin and APJ mediate a wide range of physiological actions, including angiogenesis (Cox *et al.*, 2006; Eyries *et al.*, 2008; Kasai *et al.*, 2008; Kidoya *et al.*, 2008), heart contractility, blood pressure regulation (Dai *et al.*, 2006) and other effects (Sorhede Winzell *et al.*, 2005; Lambrecht *et al.*, 2006; Lago *et al.*, 2007). Apelin and APJ are expressed on ECs of newly developing blood vessels during angiogenesis (Kidoya *et al.*, 2008), and it has been reported that apelin expression is induced by hypoxia in ECs (Eyries *et al.*, 2008). *In vitro* analyses revealed that apelin stimulates the proliferation, migration and tube formation of ECs (Kasai *et al.*, 2004; Masri *et al.*, 2004). Recently, we reported that apelin-deficient mice have narrow blood vessels, but in contrast, apelin-overexpressing mice have enlarged blood vessels. Apelin induces larger cords of ECs, mainly mediated by cell–cell aggregation, resulting in the formation of enlarged blood vessels (Kidoya *et al.*, 2008). These enlarged blood vessels are stable, and vascular permeability was reduced (Kidoya *et al.*, 2010). Taken together, these data support the notion that the apelin/APJ pathway has an important role in vascular maturation, especially for regulating the caliber of blood vessels to facilitate lumen enlargement (Kasai *et al.*, 2008; Kidoya *et al.*, 2008).

Correspondence: Professor N Takakura, Department of Signal Transduction, Research Institute for Microbial Diseases, Osaka University, 3-1 Yamada-oka, Suita, Osaka 565-0871, Japan.
E-mail: ntakaku@biken.osaka-u.ac.jp
[4]These authors contributed equally to this work.
Received 24 July 2011; revised 3 September 2011; accepted 19 September 2011; published online 31 October 2011

Invariant natural killer T (iNKT) cells are implicated in the control of autoimmunity (Singh *et al.*, 2001), resistance to tumors (Shin *et al.*, 2001; Smyth *et al.*, 2002) and protection against infectious agents (Kakimi *et al.*, 2000). The iNKT cells are characterized by the co-expression of natural killer (NK) receptor and T-cell receptor (TCR), which is encoded in humans by Vα24-JαQ gene segments and in mice by homologous Vα14-Jα281 sequences (Taniguchi *et al.*, 2003). iNKT cells are activated by a specific glycolipid antigen α-galactosylceramide (αGalCer) presented on CD1d (Kawano *et al.*, 1997; Brossay *et al.*, 1998; Spada *et al.*, 1998). Activated iNKT cells also induce cell death in tumor cells by the expression of a wide variety of cell death-inducing effector molecules, including perforin, Fas ligand and tumor necrosis factor-related apoptosis-inducing ligand, in a manner similar to other cytotoxic cells such as NK cells and CD8 cytotoxic T cells (Nieda *et al.*, 2001). Furthermore, activation of iNKT cells induces a rapid release of cytokines, including interleukin-4, interleukin-12 and interferon-γ (IFN-γ) (Smyth *et al.*, 2002).

We previously reported that intravenous injection of αGalCer-pulsed dendritic cells (DCs) induced the activation of murine iNKT cells *in vivo*, and eradicated established metastatic tumor foci in models of mouse liver and lung metastasis (Shin *et al.*, 2001). Based on these observations in murine models, several clinical trials of intravenous injection of αGalCer-pulsed DCs have been performed (Nieda *et al.*, 2001; Motohashi *et al.*, 2009). In these studies, the interventions had limited clinical efficacy in advanced cancer patients, although iNKT cell-specific systemic immune responses had been induced in a large population of the patients. We hypothesized that optimal delivery of effector cells to the target tissues is necessary to improve the efficacy of this immunotherapy. Therefore, we performed a clinical trial using intra-arterial infusion of activated iNKT cells for patients with advanced head and neck cancer (Kunii *et al.*, 2009), and a significant tumor reduction was observed in some patients after direct infusion of iNKT cells to the tumor-feeding arteries.

In the present study, we analyze the expression and function of the apelin–APJ system in the tumor vasculature and examined the therapeutic effects of apelin-mediated tumor vascular normalization. Moreover, we also studied the effects of combination therapy with tumor vascular normalization by apelin and cancer immunotherapy by activated DC transplantation in the mouse tumor model.

## Results

*Apelin and APJ are highly expressed in tumor ECs*

We previously reported temporal expression of APJ in ECs during angiogenesis in embryos and during the process of recovery from ischemic states (Kidoya *et al.*, 2008, 2010). To determine whether apelin and APJ are expressed in a cell type-specific manner in ECs of tumor vessels, we evaluated the expression of vascular apelin and APJ in growing syngeneic mouse tumors by real-time PCR and immunohistochemical analyses. In real-time PCR analysis, we used CD31+ CD45− ECs obtained from the heart, skin or tumors of mice by fluorescence-activated cell sorting sorting. Compared with normal tissue ECs, APJ was more highly expressed in ECs from colon26 murine colon adenocarcinoma and Lewis lung carcinoma (LLC) (Figure 1a).

Immunohistochemical analysis of tumor tissue derived from colon26 murine colon cancer revealed that apelin and APJ are specifically expressed in the tumor vasculature (Figures 1b and c). Apelin and APJ expression was not observed in all tumor vessels, but about 13% of vessels were APJ-positive and about 27% of vessels were apelin-positive (Figure 1d). By analyzing the relationship between location or caliber of vessels and APJ expression, many APJ-positive ECs were observed in the large-caliber blood vessels in the peripheral region (Figure 1e). We also detected apelin and APJ protein expression in LLC tumor tissue blood vessels by immunohistochemical staining (Figures 1f and g). In these tumors, most ECs co-expressed apelin and APJ as reported previously (Kälin *et al.*, 2007) (data not shown). These data indicated that apelin and APJ are highly expressed in tumor blood vessels.

*Apelin induces blood vessel enlargement in tumors and inhibits tumor growth*

To analyze the effects of apelin on the morphology of blood vessels, we first observed the growth of blood vessels in tumors. Colon26 mouse colon cancer cells stably transfected with the apelin expression vector (Figure 2a) were inoculated under the skin of BALB/c mice to form tumors. Overexpression of apelin greatly inhibited the growth of colon26 tumors in all three cell lines derived from distinct clones (Figure 2b). In agreement with a previous report that apelin induced enlarged blood vessels in the dermis of apelin Tg mice (Kidoya *et al.*, 2010), the caliber of blood vessels observed in tumors formed by colon26 cells transduced with apelin was enlarged compared with control colon26 tumors (Figures 2c–e). This enlargement of tumor vessels is not dependent on tumor size, because the lumen size of the vessels was different even for tumors of the same volume (300 $mm^3$) (Supplementary Figure 1; day 8 for colon26/vector, day 10 for colon26/apelin). However, there is little difference between density of blood vessels in apelin-expressing tumor and control tumor (date not shown). Blood vessel enlargement by apelin was also observed in tumors developed from PC3 human prostate cancer cells (Figures 2f–h) and B16 mouse melanoma cells (data not shown). This indicated that the action of apelin on the change in the caliber of blood vessels is not a specific response to colon26 cells.

It is well known that the size of newly developed blood vessels is affected by mural cell adhesion to ECs during the maturation process of blood vessel formation (Gerhardt and Betsholtz, 2003). Usually, the blood vessels observed in tumors are not well covered with mural cells. In order to determine whether apelin is

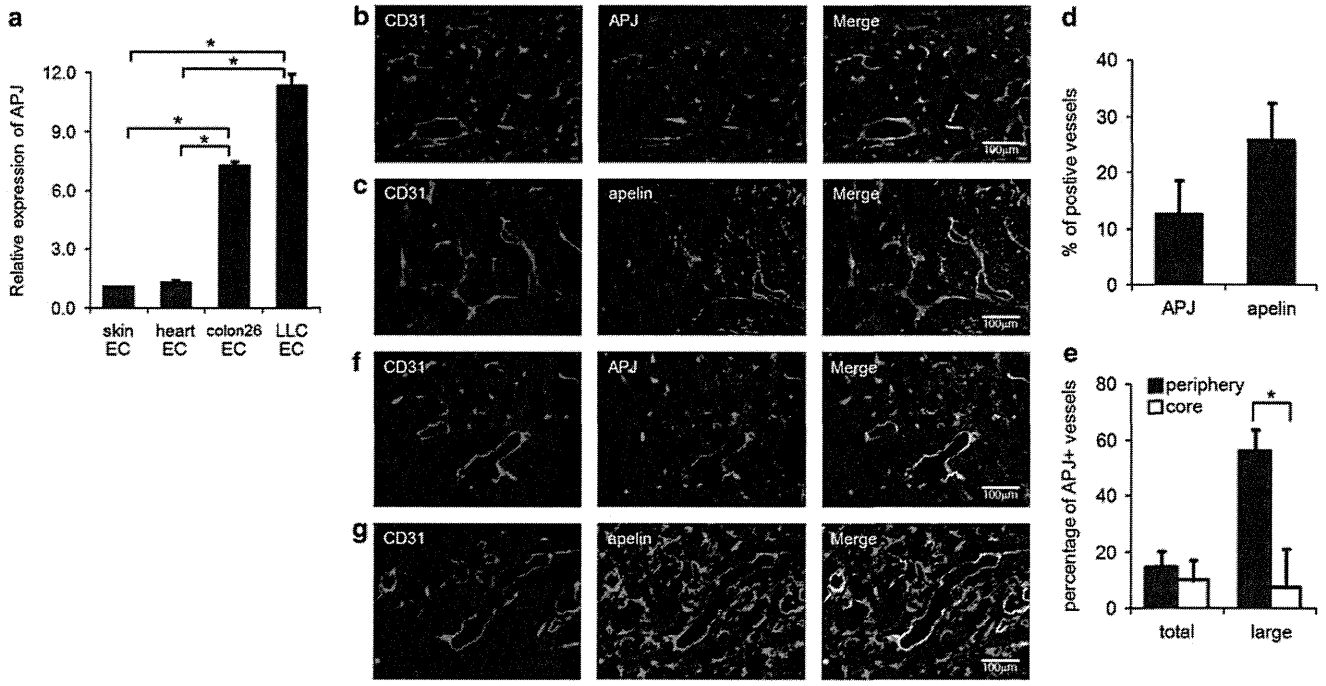


**Figure 1** Analysis of apelin and APJ expression in ECs of the tumor vasculature. (**a**) Quantitative real-time PCR analysis of APJ mRNA expression in CD31+CD45− ECs derived from mouse skin and heart, and colon26 or LLC tumors 12 days after implantation. $^*P<0.01$. (**b**, **c**) Immunohistochemical staining of sections from colon26 tumors using anti-CD31 (red) and anti-APJ (green) antibodies (**b**) or anti-apelin (green) antibodies (**c**). The scale bar indicates 100 μm. (**d**) Quantification of the ratio of tumor vessels expressing apelin or APJ. The data represent the ratio of apelin- or APJ-positive vessels versus apelin- or APJ-negative vessels as determined by immunohistochemical analysis. (**e**) Quantification of the size of APJ-positive blood vessels and their localization in colon26 tumors by immunohistochemical analysis. $^*P<0.01$. (**f**, **g**) Immunohistochemical staining of tumor sections from LLC tumors using anti-CD31 (red) and anti-APJ (green) antibodies (**f**), or anti-apelin (green) antibodies (**g**). The scale bar indicates 100 μm.

involved in muscularization resulting in enlargement of blood vessels, tumor sections were stained with an anti-smooth muscle actin antibody. As shown in Figure 2i, the preexisting vessels around tumor were well muscularized, but mural cells did not adhere to the ECs of enlarged blood vessels in colon26 tumors expressing apelin. This suggested that the induced enlargement of blood vessels by apelin occurs independently of mural cells.

*Apelin induces the formation of functional, non-leaky, mature vessels*

Recent reports indicate that anti-angiogenic cancer therapy often converts the immature blood vessels in tumors to more a normal functional vascular network (Jain, 2005; Dickson *et al.*, 2007). As shown Figure 2b, apelin-mediated maturation of the tumor vasculature suppressed tumor growth. Therefore, we examined whether the apelin-induced enlargement of blood vessel also contributes to functional blood vessel normalization. Because the tumor vasculature is generally immature and leaky, oxygen cannot reach the center of the tumor tissue, leading to hypoxia. However, the hypoxic status of the center of tumor tissues was moderated in the tumors formed by the colon26 cells transduced with apelin (Figures 3a and b). Moreover, fluorescence-conjugated 100 mM dextran effectively infiltrated to the center of tumor tissues in apelin-expressing colon26 tumors (Figures 3c and d). These results indicate that the apelin-mediated enlargement of tumor vessels also induced the functional maturation of the blood vessels.

We then analyzed the phenotype of the CD31+CD45− ECs isolated from apelin-expressing or control colon26 tumors. In the apelin-transduced tumors, the expression level of EC-related genes VCAM1, Flk1, Flt1 and APJ was increased (Figures 3e and f). Furthermore, consistent with our previous report, expression of the EC junction proteins VE-cadherin and Claudin5 was upregulated (Figure 3f). Therefore, we speculated that the increased vascular stability observed in the apelin-expressing tumors is due to these changes in the EC phenotypes.

*Functional analysis of αGalCer-pulsed mature BMDCs*

Tumor vessel vascular normalization has been reported to enhance the therapeutic effects of anticancer drugs, radiotherapy and immunotherapy (Willett *et al.*, 2006). Therefore, we examined whether induction of functional normalization of blood vessels induced by apelin improved the efficacy of cancer immunotherapy. In addition, we hypothesized that vascular normalization would improve the migration of antitumor effector cells to the tumor site. Furthermore, we believed that

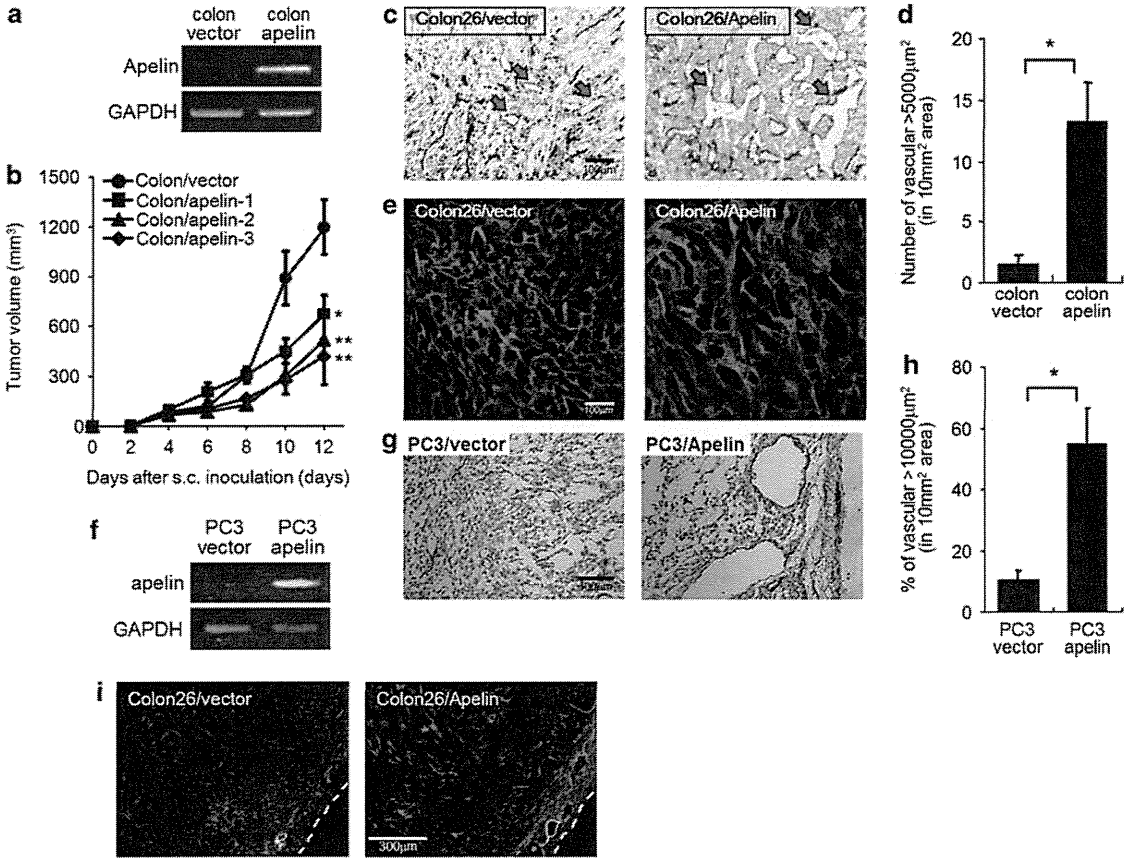


**Figure 2** Apelin induces enlargement of blood vessels in tumors and inhibits tumor growth. (**a**) Reverse transcription–PCR (RT–PCR) analysis of apelin expression in colon26 tumor cells. GAPDH was used as a positive control. (**b**) The growth curves of control and apelin-overexpressing colon26 tumors implanted in the dorsa of BALB/c mice ($n = 10$ mice per group). $^{*}P < 0.05$; $^{**}P < 0.01$ (comparison with colon/vector tumor). (**c**) Immunohistochemical staining of sections from tumors generated by colon26 cells and colon26 cells transduced with apelin. Blood vessels were stained by an anti-CD31 mAb (brown). The arrows indicate typical vessels. Scale bar, 100 μm. (**d**) The number of enlarged blood vessels having a $> 5 \times 10^3$ μm² luminal cavity per 10-mm² area was quantitatively evaluated in each tumor section. $^{*}P < 0.001$. (**e**) Confocal imaging of 50-μm sections from tumors generated from colon26 cells or colon26 cells transduced with apelin. Sections were stained by an anti-CD31 mAb. (**f**) RT–PCR analysis of apelin expression in PC3 tumor cells. GAPDH was used as a positive control. (**g**) Immunohistochemical staining of sections from tumors generated from PC3 cells or PC3 cells transduced with apelin. Sections were stained by an anti-CD31 mAb (brown). Scale bar, 100 μm. (**h**) The number of enlarged blood vessels having a $> 10^4$ μm² luminal cavity per 10-mm² area was quantitatively evaluated in each tumor section. $^{*}P < 0.001$. (**i**) Immunohistochemical staining of sections from control colon26 tumors or apelin-overexpressing colon26 tumors using an anti-CD31 antibody (green) and an anti-α-smooth muscle actin antibody (red). Scale bar, 300 μm.

effector cell-mediated cancer immunotherapy, combined with vascular normalization, would demonstrate more significant antitumor effects than either treatment alone.

iNKT cells are a very small cell population in the peripheral blood before stimulation with αGalCer, a specific glycolipid antigen (Kawano *et al.*, 1997; Brossay *et al.*, 1998; Spada *et al.*, 1998). After activation, the iNKT cell population significantly expands and exerts strong antitumor activity against various malignant tumors both *in vivo* and *in vitro* (Kawano *et al.*, 1999; Shin *et al.*, 2001; Seino *et al.*, 2005). Therefore, we investigated the synergistic effects between vascular normalization with apelin and immunotherapy with αGalCer-pulsed DCs whose antitumor response had already reported in mice and humans (Nieda *et al.*, 2004; Kunii *et al.*, 2009; Motohashi *et al.*, 2009).

Prepared αGalCer-pulsed or vehicle-pulsed mature bone marrow (BM)-derived DCs (BMDCs) were analyzed by flow cytometry after 8 days of culture. Both groups of BMDCs highly expressed CD11c (83%) and major histocompatibility complex (MHC) class-II (about 95%); moreover, the expression levels of CD86 and CD80 were also high (60–90%) (Figure 4a). These cells were injected into mice on day 0 and then the number of peripheral iNKT cells was monitored. The iNKT cell populations were significantly elevated on day 4 in mice injected with αGalCer-pulsed BMDCs (Figure 4b). Alternately, peripheral iNKT cell numbers remained at low levels in mice injected with vehicle-pulsed DCs. Therefore, we used both sets of DCs for antitumor immunotherapy experiments.

### *Enhancement of antitumor effects by combination of apelin stimulation and DC treatment*

To evaluate the synergistic effect of apelin-mediated normalization of the tumor vasculature and immu-

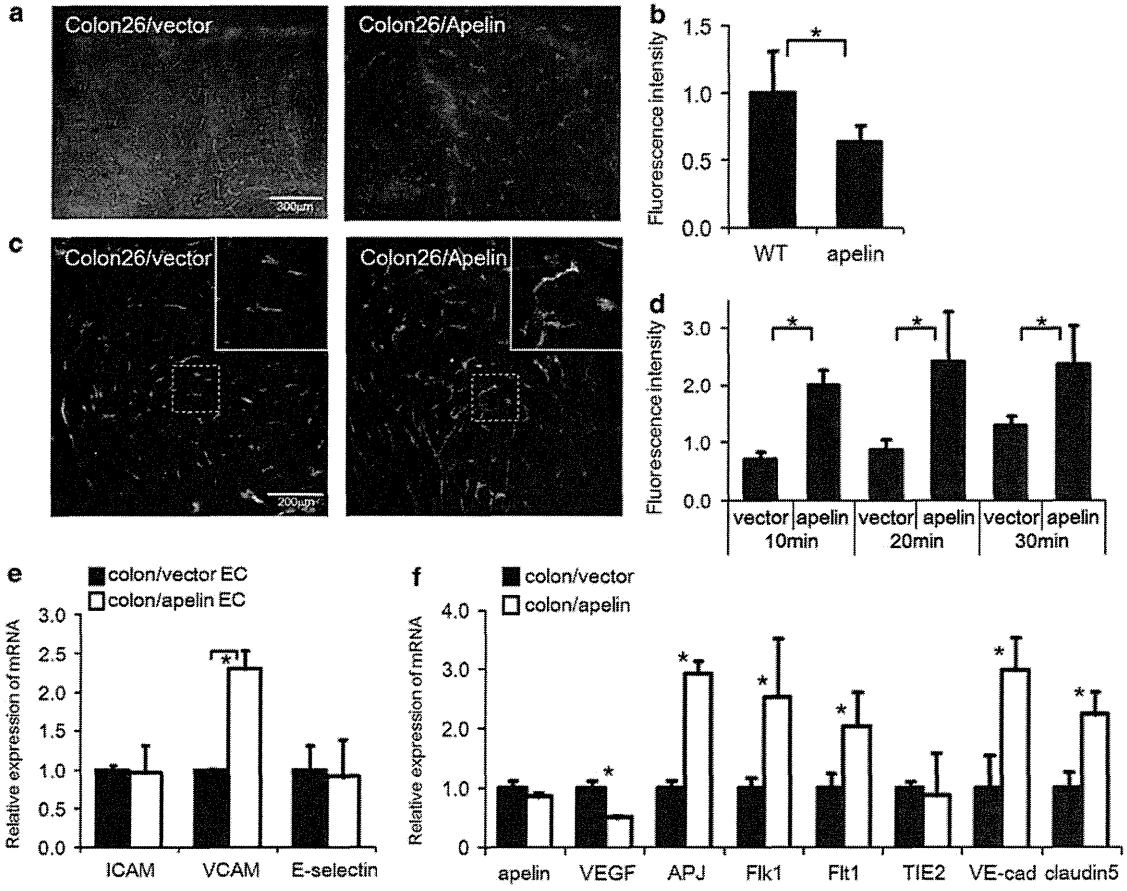


**Figure 3** Apelin induces the formation of functional, non-leaky, mature vessels. (**a**) Colon26 control and apelin-overexpressing tumors were stained for CD31 (red) and hypoxia (HypoxyProbe, green). Scale bar, 100 μm. (**b**) The hypoxic region within the vascularized tumor was quantified by the fluorescence intensity in HypoxyProbe staining. $^*P<0.01$. (**c**) Microscopy images of fluorescein isothiocyanate–dextran angiography and the vasculature (CD31, red) on colon26 control and apelin-overexpressing tumors. Scale bar, 100 μm. (**d**) Time-course analysis of the fluorescence intensity of extravascular fluorescein isothiocyanate–dextran as a measure of vascular permeability. $^*P<0.01$. (**e**, **f**) Quantitative real-time RT–PCR analysis for cell adhesion molecules (**e**) or EC-related factors (**f**) using total RNA for CD31 + CD45− ECs isolated by cell sorting from colon26 control and apelin-overexpressing tumors. $^*P<0.01$.

notherapy with mature DCs, we analyzed the antitumor activity of the combination therapy. Development of the tumor vasculature was observed between 4 and 6 days after implantation of colon26 cells (Supplementary Figure 2). Therefore, after implantation of colon26/vector or colon26/apelin cells into the subcutaneous tissue of mice, mature DCs were administered by intravenous injection on day 4 and tumors were harvested on day 14 (Figure 5a). We observed antitumor effects, as described previously, in the apelin-expressing tumor or in vector-transduced colon26 tumors treated with αGalCer/DCs, but more remarkable antitumor effects were observed in mice that underwent both apelin transduction and DC treatment (Figures 5b–d). Growth of colon26/apelin tumors treated with αGalCer/DCs slowed when tumor volumes exceeded 100 $mm^3$ (Figure 5b). The tumor weight of colon26/apelin tumors treated with αGalCer/DCs was exceedingly small and comprised only about a fourth of the vehicle/DCs-treated, apelin-transduced colon26 tumors or αGalCer/DCs-treated, vector-transduced colon26 tumors (Figures 5c and d). These data suggest that the vascular normalization induced by apelin markedly improved the effects of immunotherapy.

To exclude the possibility that apelin activated the immune cells and enhanced their antitumor effect, we analyzed the expression of APJ in iNKT cells and DCs. Compared with tumor blood vascular ECs, APJ expression in iNKT cells and in each of the DCs was extremely low and almost undetectable, respectively (Figure 5e). Therefore, apelin is not likely to directly activate these cells.

*Infiltration of iNKT cells into tumor tissues was promoted by apelin-induced vascular maturation*

Finally, to confirm that the antitumor effect observed in the colon26/apelin tumors treated with αGalCer/DCs was actually caused by iNKT cell infiltration into tumor tissue or activation induced by the DCs, we analyzed tumor tissues, which were harvested 14 days after tumor cell inoculation. We observed higher levels of NKp46 + cell infiltration in αGalCer/DC-treated colon26/apelin tumors as compared with colon/vector tumors and

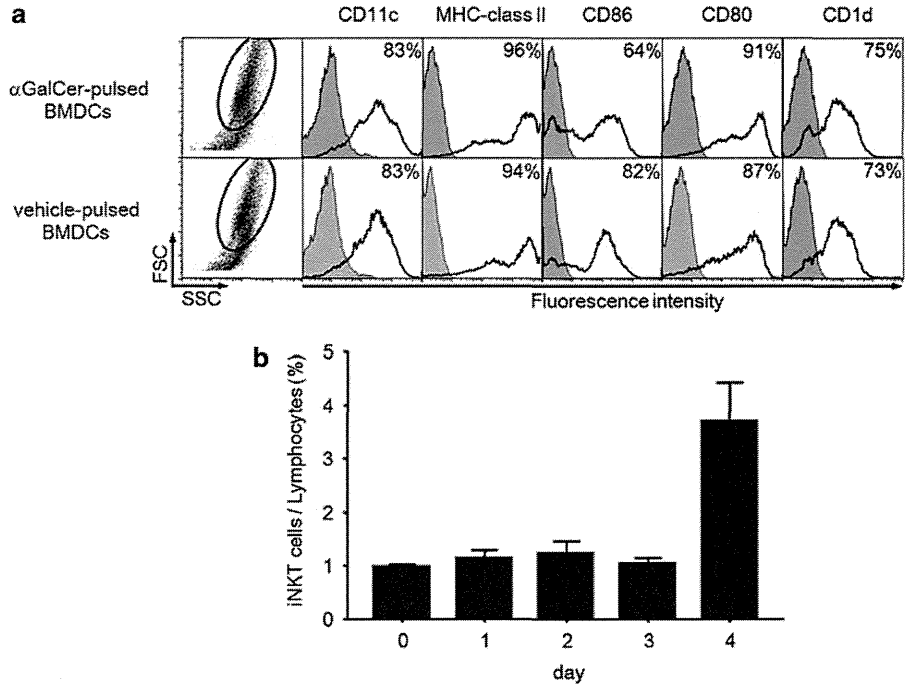


**Figure 4** Functional analysis of αGalCer-pulsed mature BMDCs. (**a**) Flow-cytometric analysis of αGalCer- or vehicle-pulsed mature BMDCs. The expression levels of CD11c, human leukocyte antigen class-II, CD86, CD80 and CD1d were assessed at the time of administration. Thin lines: background staining with an isotype-matched control; bold line: staining profiles of the indicated molecules. (**b**) The percentage of peripheral blood iNKT cells (TCR-β + αGalCer-CD1d-tetramer + cells) after injection of αGalCer-pulsed mature BMDCs ($6 \times 10^5$ cells) was assessed by flow-cytometric analysis.

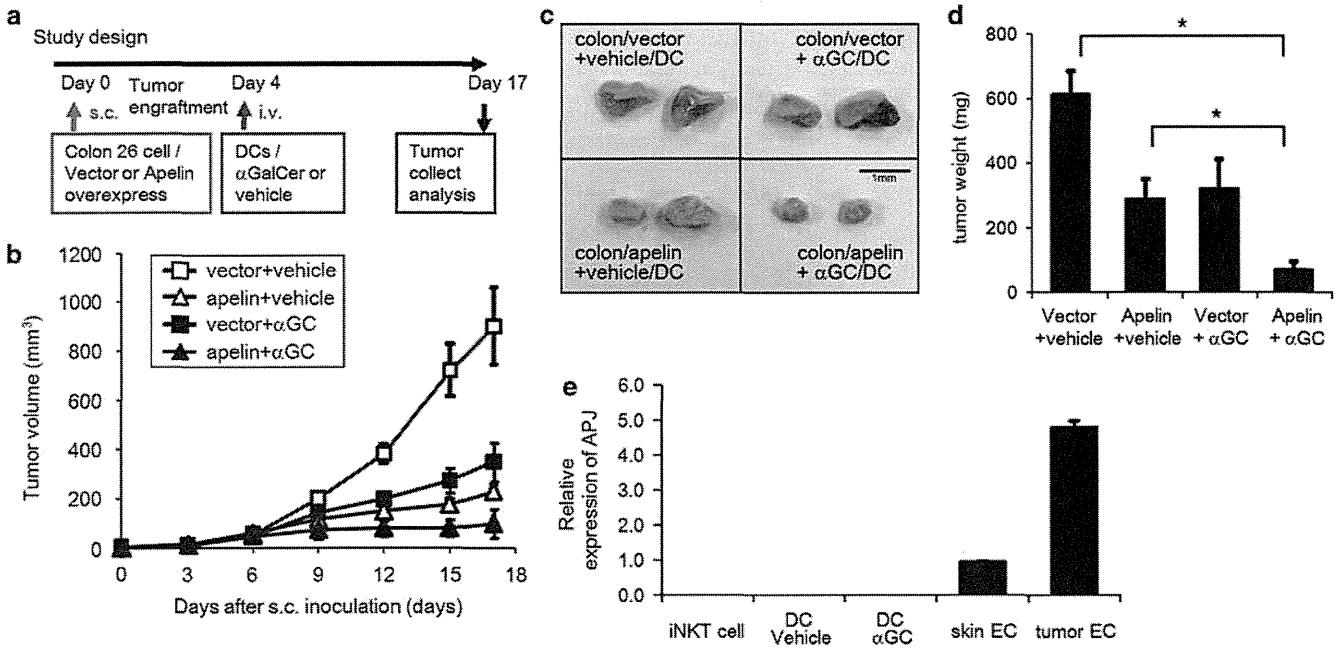


**Figure 5** Enhancement of the antitumor effect by combination of apelin stimulation and DC treatment. (**a**) A schematic diagram of the experimental protocol of tumor isograft and DC treatment assays. (**b**) Growth curves of control and apelin-overexpressing colon26 tumors implanted in the dorsa of BALB/c mice treated with control vehicle-pulsed DCs or αGalCer-pulsed DCs ($n = 10$ mice per group). (**c**) Representative pictures of tumors collected 15 days after subcutaneous inoculation. Scale bar, 1 mm. (**d**) Tumor volume was determined on day 15 after subcutaneous inoculation of each tumor. $^*P < 0.01$. (**e**) Quantitative real-time RT–PCR analysis of APJ mRNA in iNKT cells and DCs. The results are shown as fold increase in comparison with the basal levels of normal ECs.

untreated tumors (Figure 6a). Consistent with this result, flow-cytometric analysis of αGalCer/DCs-treated colon/apelin tumors showed significant augmentation of iNKT cells (TCR-β + αGalCer-CD1d-tetramer + ) in tumor tissues as compared with those in the untreated tumors (Figures 6b and c).

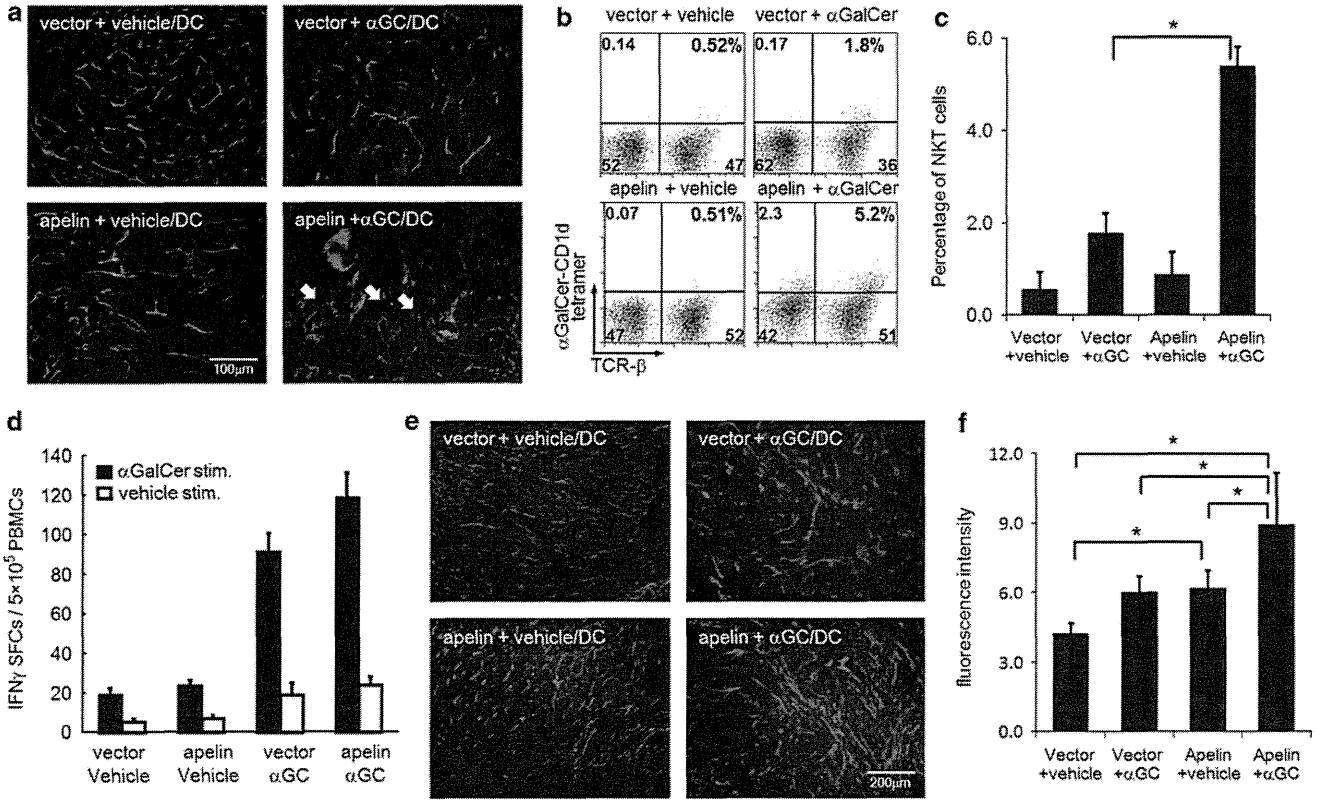


**Figure 6** Infiltration of iNKT cells into tumor tissues was promoted by apelin-induced vascular maturation. (**a**) Immunohistochemical staining of sections from control and apelin-overexpressing colon26 tumors treated with control vehicle-pulsed DCs or αGalCer-pulsed DCs. Sections were stained by using anti-NKp46 (red) and anti-CD31 antibodies (green). Scale bar, 100 μm. (**b**) Flow-cytometric analysis of tumor-infiltrating CD45-positive lymphocytes. Cells were stained by a αGalCer-loaded CD1d tetramer and an anti-TCR-β antibody. (**c**) Quantitative evaluation of the percentage of iNKT cells (αGalCer-CD1d-tetramer + TCR-β + CD45 + iNKT cells/CD45 + lymphocytes) in tumor-infiltrating lymphocytes with s.d. $^*P<0.01$. (**d**) The mean number of IFNγ spot-forming cells with s.d., determined by ELISpot assay. A total of $5\times10^5$ peripheral blood mononuclear cells were stimulated for 16 h with αGalCer or vehicle *in vitro*. The mean numbers of IFN-γ spots were determined from triplicate cultures. (**e**) Apoptosis of tumor cells was detected by the TUNEL method (green) and blood vessels were stained with an anti-CD31 antibody (red). Scale bar, 200 μm. (**f**) Quantification of apoptosis in tumor sections by measurement of fluorescence intensity of TUNEL-positive cells. $^*P<0.01$.

IFN-γ production in response to αGalCer antigenic stimulation was increased in peripheral blood cells of mice treated with αGalCer/DCs (Figure 6d). Moreover, many apoptotic tumor cells were observed in αGalCer/DC-treated colon26/apelin tumors (Figures 6e and f). These results suggest that the potent antitumor effects observed in αGalCer/DC-treated colon26/apelin tumors was caused by enhanced infiltration of iNKT cells in the center of the tumor tissue, thus inducing apoptotic tumor cell death.

## Discussion

We found that expression of APJ (the apelin receptor) was significantly increased in tumor blood vessels and apelin simulation induced enlargement of the caliber of tumor vessels. Enlargement of tumor vessels by apelin also led to functional maturation and normalization, including suppression of vascular permeability and improvement of oxygen supply to the central tumor.

Normalization of the tumor vasculature induced by VEGF-neutralizing antibodies has been reported to suppress tumor growth (Kim *et al.*, 1993). In our study, apelin-induced vascular maturation also demonstrated an antitumor growth effect. One of the major therapeutic benefits of tumor vascular normalization is enhancement of the effects of conventional cancer therapy such as chemotherapy, radiotherapy and immunotherapy. In our present study, we used a combination of immunotherapy with DC treatment with vascular normalization therapy due to apelin expression and obtained remarkable antitumor effects. These therapeutic effects resulted from induction of tumor cell apoptosis by effective infiltration of activated iNKT cells.

Several researchers have reported that apelin is relevant to blood vessel formation not only under physiological conditions, but also in a neoplastic context (Seaman *et al.*, 2007; Sorli *et al.*, 2007). Consistent with these results, we found that apelin expression was observed in vascular ECs of colon26 tumors and LLC tumors. In addition, we revealed that APJ expression was also upregulated in these tumor ECs. Our previous

report showed that APJ expression was induced by VEGF stimulation of ECs of blood vessels where angiogenesis is taking place (Kidoya *et al.*, 2008).We predict that APJ expression in tumor blood vessels is also regulated by the same mechanism, because angiogenesis is frequently observed in tumor tissues. Of interest, APJ-expressing angiogenic ECs are almost imperceptible in healthy adults. Although apelin has been reported to act on heart contractility and blood pressure regulation, apelin-deficient and apelin-overexpressing mice show normal growth after birth (Kidoya *et al.*, 2008, 2010). Therefore, anti-angiogenesis drugs targeting apelin would be expected to have fewer side effects than other anti-angiogenic agents targeting more ubiquitously expressed molecules such as VEGF.

We previously reported that apelin regulates the lumen size of the blood vessels of embryos during the vascular maturation process. In this report, we found that the tumor vasculature is also regulated by apelin stimulation. Blood vessels in tumors are functionally immature and characteristically leaky in nature (Bergers and Benjamin, 2003). From analysis of blood vessels in the skin of apelin-overexpressing mice, it was apparent that apelin can enhance vascular stability and suppress vascular permeability (Kidoya *et al.*, 2010). In the tumor vessels examined in our present study, we found that apelin improved stability and induced normalization by upregulating the expression of adhesion molecules in ECs.

Tumor blood vessels are structurally and functionally abnormal, and these abnormalities impair the tumor oxygen supply (Padera *et al.*, 2004). The hypoxic microenvironment formed in this manner induces genetic instability and leads to further alterations in malignant cells (Bottaro and Liotta, 2003). The vascular normalization induced by a VEGF-neutralizing antibody can alleviate the hypoxic condition of the tumor microenvironment and suppress malignant transformation. Apelin stimulation also improved the function of tumor blood vessels and alleviated the hypoxia. We attributed the growth suppression of the apelin-expressing tumors observed in this study to this effect. It is possible that tumor vessels normalized by apelin enhance the delivery of nutrients to tumor cells. However, this vascular normalization might also induce an antitumor effect by immunocyte infiltration, because the concentration of apoptotic tumor cells was increased in the colon/apelin + vehicle group as compared with the colon/vector + vehicle group, as shown in Figure 6f.

Contrary to our results, it has been reported that apelin induces tumor angiogenesis and promotes tumor growth (Sorli *et al.*, 2007). This difference might depend on the particular apelin–APJ signaling pathway that has been activated, such as the angiopietin1–Tie2 signaling pathway (Fukuhara *et al.*, 2008). The apelin–APJ system activates the Akt and ERK (extracellular-signal regulated kinase) signaling pathways, which might be involved in vascular stabilization and pro-angiogenesis, respectively. Therefore, apelin may have a beneficial effect in cancer treatment, if it can be predicted before treatment in individual cases that apelin induces normalization of the tumor vasculature.

Current immunotherapy for human solid cancers can be classified into the following categories (Rosenberg *et al.*, 2008): one is non-specific immunomodulation, such as interleukin-2 therapy for renal cancer or metastatic melanoma (Rosenberg *et al.*, 1989). Another is use of a cancer vaccine containing tumor peptides or DCs (Steinman and Banchereau, 2007) that activates the patient's immunity against their cancer. The last category is adoptive cell transfer, in which *in vitro* expanded autologous antitumor effector cells are administered to the patient (Rosenberg *et al.*, 2008). In all of these treatments, effector cell delivery to the tumor site is indispensable, and therefore, improvements in delivery would increase the therapeutic effects of all of these approaches. In this study, we used the DC therapy targeted to iNKT cells because tumor-infiltrating cells can be specifically evaluated. There are few iNKT cells at the tumor site before stimulation, and significant expansions of iNKT cells were observed after activation with the unique antigen. Based on these findings, it was strongly expected that combination with vascular normalization therapy would also improve the efficacy of the other immunotherapy such as tumor antigen-specific T-cell therapy. Therefore, as a follow-up study, we are preparing to examine combination treatment by adoptive cell transfer using engineered T lymphocytes (June *et al.*, 2009), and the difference in infiltration into the tumor site between iNKT cells and conventional T cells will be assessed.

Induction of vascular normalization leads to enhancement of the efficacy of conventional therapies (Willett *et al.*, 2006). Here we have demonstrated that combination therapy using vascular maturation induced by apelin and immune therapy with administration of antigen-loaded DCs remarkably suppressed the growth of colon26 tumors. This antitumor effect was attributed to dramatic infiltration of DC-activated iNKT cells and subsequent induction of apoptosis in the tumor cells. It was recently reported that inhibition of angiogenesis lead to normalized endothelial adhesion molecule levels and improves tumor growth inhibition by promoting leukocyte extravasation (Dings *et al.*, 2011). Upregulation of VCAM1 expression was also induced in the endothelium of apelin-expressing tumor, and it would promote iNKT cell infiltration. Tumor vascular normalization induced by apelin therefore appears to augment immunotherapy as well as chemotherapy and radiotherapy.

In summary, our data suggest that vascular normalization induced by apelin can enhance the effect of immunotherapy by promoting immune cell recruitment. Many angiogenic factors have been identified, and their functions have been described, and many of these factors have been or are being targeted as new cancer therapy approaches. Compared with these angiogenic molecules, apelin has a unique function in that it regulates blood vessel maturation, but has limited functions with regard to induction of angiogenesis. In addition, apelin-targeting agents would have fewer side effects, because expression of the apelin receptor, APJ, is confined to newly formed blood vessels such as tumor

vessels. Induction of tumor vascular normalization by recombinant apelin administration is difficult because the apelin peptide is unstable. For these reasons, the design of drugs that target the apelin–APJ system, such as more stable and potent APJ receptor agonist, is expected to provide novel agents that by regulating the tumor vasculature will introduce an effective new cancer treatment.

## Materials and methods

*Mice*
C57BL/6 mice, KSN nude mice and BALB/c mice at 8 weeks of age were purchased from Japan SLC (Shizuoka, Japan) and were used between 8 and 12 weeks of age. The animals were housed in environmentally controlled rooms of the animal experimentation facility at Osaka University. All experiments were performed in compliance with the laws and institutional guidelines of Osaka University.

*Cells*
Cell lines, including colon26, PC3 and LLC, were purchased from RIKEN cell bank (Tsukuba, Japan). The culture medium used was RPMI-1640 containing 10% fetal calf serum, 50 μM 2-mercaptoethanol, 2 mM glutamine and 10 mM HEPES buffer. DCs were grown from bone marrow progenitors in culture medium supplemented with 20 ng/ml recombinant murine granulocyte–macrophage colony-stimulating factor (eBioscience, San Diego, CA, USA) (Fujii *et al.*, 2002). On day 6, αGalCer (100 ng/ml; Kyowa Hakko, Gunma, Japan) was added to immature BMDCs for 40 h. To induce maturation of the DCs, 100 ng/ml lipopolysaccharide (Wako, Osaka, Japan) was added on day 7 for 16 h. Mature αGalCer-pulsed DCs were collected on day 8.

*Tissue preparation, immunohistochemistry and flow cytometry*
Tissue fixation and staining of sections with antibodies were performed as described previously (Takakura *et al.*, 2000). An anti-CD31 monoclonal antibody (mAb) (BD Biosciences, San Diego, CA, USA), anti-α-smooth muscle actin mAb (Dako, Glostrup, Denmark), anti-apelin mAb (4G5) (Kawamata *et al.*, 2001), anti-APJ polyclonal Ab (Kidoya *et al.*, 2008) and an anti-NKp46 mAb (R&D Systems, Minneapolis, MN, USA) were used for staining. TUNEL (TdT-mediated dNTP nick end labeling) assays were performed using the ApopTag Plus kit (Millipore, Billerica, MA, USA). Sections were observed by conventional microscopy (DM5500 B; Leica, Wetzlar, Germany) or confocal microscopy (TCS/SP5; Leica), and images were acquired with a digital camera (DFC500; Leica). In all assays, an isotype-matched control Ig was used as negative control and it was confirmed that the positive signals were not derived from nonspecific background. Images were processed using the Photoshop CS2 software (Adobe Systems, San Jose, CA, USA). Flow-cytometric analysis was performed as described previously (Yamada and Takakura, 2006). Fluorescence-labeled anti-CD45, anti-CD31, anti-CD86, anti-MHC class-II, anti-TCR-β, anti-CD1d, anti-CD80, anti-CD11c antibody (BD Biosciences) and CD1d tetramer antibodies (Proimmune, Oxford, UK) were used. Stained cells were analyzed with a FACSCalibur (BD Biosciences), by using the FlowJo software (TreeStar, Ashland, OR, USA), and sorted by using a JSAN flow cytometer (Bay Bioscience, Kobe, Japan). Dead cells were excluded from propidium iodide staining or analyses using the two-dimensional profile of the forward versus side scatter.

*Real-time PCR analysis*
Total RNA was extracted by using the RNeasy plus kit (Qiagen, Hilden, Germany) and reverse-transcribed into cDNA using the ExScript RT-PCR kit (Takara, Otsu, Japan). The primer pairs used for analysis are listed in Supplementary Table 1. Real-time PCR analysis was performed by using Platinum SYBR-Green SuperMix-UDG (Invitrogen, Carlsbad, CA, USA). The levels of PCR products were monitored with an Mx3000P QPCR system (Agilent, Santa Clara, CA, USA). Baseline and threshold were adjusted according to the manufacturer's instructions. The relative abundance of transcripts was normalized to the constitutive expression level of glyceraldehyde-3-phosphate dehydrogenase (GAPDH) RNA.

*Tumor growth assay*
The mouse *Apelin* gene was cloned into the pCAGSIH expression vector (Kidoya *et al.*, 2008). Colon26 cells and PC3 cells were stably transfected by using the Lipofectamine Plus reagent (Invitrogen) and clones of cells showing stable transfection were obtained by antibiotic resistance selection using G418 (Gibco, Grand Island, NY, USA) and hygromycin-B (Sigma, St Louis, MO, USA). The stably transfected colon26 clones ($1 \times 10^6$ cells), PC3 clones ($1 \times 10^7$ cells) or LLC cells ($3 \times 10^6$ cells) were inoculated subcutaneously into 6- to 8-week-old BALB/c mice, nude mice or C57BL/6 mice, respectively, and tumors were dissected at 12–15 days after implantation. DCs ($6 \times 10^5$ cells) were administered by intravenous injection 4 days after tumor implantation. To measure hypoxia in tumor tissues, HypoxyProbe-1 (Millipore; 60 mg/kg) was injected intraperitoneally 1 h before killing. Tumors sections were stained using an anti-HypoxyProbe antibody. To evaluate macromolecule infiltration, mice were intravenously injected with fluorescein isothiocyanate-conjugated dextran (500 μg; Vector Laboratories, Burlingame, CA, USA) and dextran was circulated for 10–30 min.

*ELISpot assay*
IFN-γ-producing cells were analyzed with a mouse IFN-γ ELISpot kit (Mabtech AB, Stockholm, Sweden). Peripheral blood mononuclear cells ($5 \times 10^5$ per well, 96-well plates) were stimulated by addition of 100 ng/ml αGalCer or vehicle. Concanavalin-A was used as a positive control. IFN-γ spot-forming cells were quantified objectively by using an ImmunoScan computer system and the ImmunoSpot software program (CTL, Cleveland, OH, USA).

*Statistical analysis*
All data are presented as the means ± s.d. For statistical analysis, the statcel2 software package (OMS, Saitama, Japan) was used, with analysis of variance performed on all data, followed by the Tukey–Kramer multiple comparison test. When only two groups were compared, a two-sided Student's *t*-test was used.

## Conflict of interest

The authors declare no conflict of interest.

## Acknowledgements

We thank Ms C Takeshita, Ms K Fukuhara and Ms N Fujimoto for technical assistance. *Financial support*: This work

was supported by Grant-in-Aid for Research Activity Start-up (KAKENHI 21890124) from the Japan Society for the Promotion of Science (JSPS) and Research; a grant from the Ministry of Education, Culture, Sports, Science and Technology (MEXT) of Japan; and the YASUDA Medical Foundation.

## References

Bergers G, Benjamin LE. (2003). Tumorigenesis and the angiogenic switch. *Nat Rev Cancer* **3**: 401–410.

Bottaro DP, Liotta LA. (2003). Cancer: out of air is not out of action. *Nature* **423**: 593–595.

Brossay L, Chioda M, Burdin N, Koezuka Y, Casorati G, Dellabona P *et al.* (1998). CD1d-mediated recognition of an alpha-galactosylceramide by natural killer T cells is highly conserved through mammalian evolution. *J Exp Med* **188**: 1521–1528.

Cox CM, D'Agostino SL, Miller MK, Heimark RL, Krieg PA. (2006). Apelin, the ligand for the endothelial G-protein-coupled receptor, APJ, is a potent angiogenic factor required for normal vascular development of the frog embryo. *Dev Biol* **296**: 177–189.

Dai T, Ramirez-Correa G, Gao WD. (2006). Apelin increases contractility in failing cardiac muscle. *Eur J Pharmacol* **553**: 222–228.

Dickson PV, Hamner JB, Sims TL, Fraga CH, Ng CY, Rajasekeran S *et al.* (2007). Bevacizumab-induced transient remodeling of the vasculature in neuroblastoma xenografts results in improved delivery and efficacy of systemically administered chemotherapy. *Clin Cancer Res* **13**: 3942–3950.

Dings RP, Vang KB, Castermans K, Popescu F, Zhang Y, Oude Egbrink MG *et al.* (2011). Enhancement of T-cell-mediated antitumor response: angiostatic adjuvant to immunotherapy against cancer. *Clin Cancer Res* **17**: 3134–3145.

Eyries M, Siegfried G, Ciumas M, Montagne K, Agrapart M, Lebrin F *et al.* (2008). Hypoxia-induced apelin expression regulates endothelial cell proliferation and regenerative angiogenesis. *Circ Res* **103**: 432–440.

Fujii S, Shimizu K, Kronenberg M, Steinman RM. (2002). Prolonged IFN-gamma-producing NKT response induced with alpha-galactosylceramide-loaded DCs. *Nat Immunol* **3**: 867–874.

Fukuhara S, Sako K, Minami T, Noda K, Kim HZ, Kodama T *et al.* (2008). Differential function of Tie2 at cell–cell contacts and cell-substratum contacts regulated by angiopoietin-1. *Nat Cell Biol* **10**: 513–526.

Gasparini G, Longo R, Toi M, Ferrara N. (2005). Angiogenic inhibitors: a new therapeutic strategy in oncology. *Nat Clin Pract Oncol* **2**: 562–577.

Gerber HP, Ferrara N. (2005). Pharmacology and pharmacodynamics of bevacizumab as monotherapy or in combination with cytotoxic therapy in preclinical studies. *Cancer Res* **65**: 671–680.

Gerhardt H, Betsholtz C. (2003). Endothelial-pericyte interactions in angiogenesis. *Cell Tissue Res* **314**: 15–23.

Heath VL, Bicknell R. (2009). Anticancer strategies involving the vasculature. *Nat Rev Clin Oncol* **6**: 395–404.

Hurwitz H, Fehrenbacher L, Novotny W, Cartwright T, Hainsworth J, Heim W *et al.* (2004). Bevacizumab plus irinotecan, fluorouracil, and leucovorin for metastatic colorectal cancer. *N Engl J Med* **350**: 2335–2342.

Jain RK. (2005). Normalization of tumor vasculature: an emerging concept in antiangiogenic therapy. *Science* **307**: 58–62.

June CH, Blazar BR, Riley JL. (2009). Engineering lymphocyte subsets: tools, trials and tribulations. *Nat Rev Immunol* **9**: 704–716.

Kakimi K, Guidotti LG, Koezuka Y, Chisari FV. (2000). Natural killer T cell activation inhibits hepatitis B virus replication *in vivo*. *J Exp Med* **192**: 921–930.

Kälin RE, Kretz MP, Meyer AM, Kispert A, Heppner FL, Brändli AW. (2007). Paracrine and autocrine mechanisms of apelin signaling govern embryonic and tumor angiogenesis. *Dev Biol* **305**: 599–614.

Kasai A, Shintani N, Kato H, Matsuda S, Gomi F, Haba R *et al.* (2008). Retardation of retinal vascular development in apelin-deficient mice. *Arterioscler Thromb Vasc Biol* **28**: 1717–1722.

Kasai A, Shintani N, Oda M, Kakuda M, Hashimoto H, Matsuda T *et al.* (2004). Apelin is a novel angiogenic factor in retinal endothelial cells. *Biochem Biophys Res Commun* **325**: 395–400.

Kawamata Y, Habata Y, Fukusumi S, Hosoya M, Fujii R, Hinuma S *et al.* (2001). Molecular properties of apelin: tissue distribution and receptor binding. *Biochim Biophys Acta* **1538**: 162–171.

Kawano T, Cui J, Koezuka Y, Toura I, Kaneko Y, Motoki K *et al.* (1997). CD1d-restricted and TCR-mediated activation of valpha14 NKT cells by glycosylceramides. *Science* **278**: 1626–1629.

Kawano T, Nakayama T, Kamada N, Kaneko Y, Harada M, Ogura N *et al.* (1999). Antitumor cytotoxicity mediated by ligand-activated human V alpha24 NKT cells. *Cancer Res* **59**: 5102–5105.

Kidoya H, Naito H, Takakura N. (2010). Apelin induces enlarged and nonleaky blood vessels for functional recovery from ischemia. *Blood* **115**: 3166–3174.

Kidoya H, Ueno M, Yamada Y, Mochizuki N, Nakata M, Yano T *et al.* (2008). Spatial and temporal role of the apelin/APJ system in the caliber size regulation of blood vessels during angiogenesis. *EMBO J* **27**: 522–534.

Kim KJ, Li B, Winer J, Armanini M, Gillett N, Phillips HS *et al.* (1993). Inhibition of vascular endothelial growth factor-induced angiogenesis suppresses tumour growth *in vivo*. *Nature* **362**: 841–844.

Kunii N, Horiguchi S, Motohashi S, Yamamoto H, Ueno N, Yamamoto S *et al.* (2009). Combination therapy of *in vitro*-expanded natural killer T cells and alpha-galactosylceramide-pulsed antigen-presenting cells in patients with recurrent head and neck carcinoma. *Cancer Sci* **100**: 1092–1098.

Lago F, Dieguez C, Gomez-Reino J, Gualillo O. (2007). The emerging role of adipokines as mediators of inflammation and immune responses. *Cytokine Growth Factor Rev* **18**: 313–325.

Lambrecht NW, Yakubov I, Zer C, Sachs G. (2006). Transcriptomes of purified gastric ECL and parietal cells: identification of a novel pathway regulating acid secretion. *Physiol Genomics* **25**: 153–165.

Lohela M, Bry M, Tammela T, Alitalo K. (2009). VEGFs and receptors involved in angiogenesis versus lymphangiogenesis. *Curr Opin Cell Biol* **21**: 154–165.

Masri B, Morin N, Cornu M, Knibiehler B, Audigier Y. (2004). Apelin (65-77) activates p70 S6 kinase and is mitogenic for umbilical endothelial cells. *FASEB J* **18**: 1909–1911.

Motohashi S, Nagato K, Kunii N, Yamamoto H, Yamasaki K, Okita K *et al.* (2009). A phase I–II study of alpha-galactosylceramide-pulsed IL-2/GM-CSF-cultured peripheral blood mononuclear cells in patients with advanced and recurrent non-small cell lung cancer. *J Immunol* **182**: 2492–2501.

Nieda M, Nicol A, Koezuka Y, Kikuchi A, Lapteva N, Tanaka Y *et al.* (2001). TRAIL expression by activated human CD4(+)V alpha 24NKT cells induces *in vitro* and *in vivo* apoptosis of human acute myeloid leukemia cells. *Blood* **97**: 2067–2074.

Nieda M, Okai M, Tazbirkova A, Lin H, Yamaura A, Ide K *et al.* (2004). Therapeutic activation of Valpha24+Vbeta11+ NKT cells in human subjects results in highly coordinated secondary activation of acquired and innate immunity. *Blood* **103**: 383–389.

Padera TP, Stoll BR, Tooredman JB, Capen D, di Tomaso E, Jain RK. (2004). Pathology: cancer cells compress intratumour vessels. *Nature* **427**: 695.

Rosenberg SA, Lotze MT, Yang JC, Aebersold PM, Linehan WM, Seipp CA *et al.* (1989). Experience with the use of high-dose interleukin-2 in the treatment of 652 cancer patients. *Ann Surg* **210**: 474–484; discussion 484–475.

Rosenberg SA, Restifo NP, Yang JC, Morgan RA, Dudley ME. (2008). Adoptive cell transfer: a clinical path to effective cancer immunotherapy. *Nat Rev Cancer* **8**: 299–308.

Seaman S, Stevens J, Yang MY, Logsdon D, Graff-Cherry C, St Croix B. (2007). Genes that distinguish physiological and pathological angiogenesis. *Cancer Cell* **11**: 539–554.

Seino K, Fujii S, Harada M, Motohashi S, Nakayama T, Fujisawa T *et al.* (2005). Valpha14 NKT cell-mediated antitumor responses and their clinical application. *Springer Semin Immunopathol* **27**: 65–74.

Shin T, Nakayama T, Akutsu Y, Motohashi S, Shibata Y, Harada M *et al.* (2001). Inhibition of tumor metastasis by adoptive transfer of IL-12-activated Valpha14 NKT cells. *Int J Cancer* **91**: 523–528.

Singh AK, Wilson MT, Hong S, Olivares-Villagomez D, Du C, Stanic AK *et al.* (2001). Natural killer T cell activation protects mice against experimental autoimmune encephalomyelitis. *J Exp Med* **194**: 1801–1811.

Smyth MJ, Crowe NY, Pellicci DG, Kyparissoudis K, Kelly JM, Takeda K *et al.* (2002). Sequential production of interferon-gamma by NK1.1(+) T cells and natural killer cells is essential for the antimetastatic effect of alpha-galactosylceramide. *Blood* **99**: 1259–1266.

Sorhede Winzell M, Magnusson C, Ahren B. (2005). The apj receptor is expressed in pancreatic islets and its ligand, apelin, inhibits insulin secretion in mice. *Regul Pept* **131**: 12–17.

Sorli SC, Le Gonidec S, Knibiehler B, Audigier Y. (2007). Apelin is a potent activator of tumour neoangiogenesis. *Oncogene* **26**: 7692–7699.

Spada FM, Koezuka Y, Porcelli SA. (1998). CD1d-restricted recognition of synthetic glycolipid antigens by human natural killer T cells. *J Exp Med* **188**: 1529–1534.

Steinman RM, Banchereau J. (2007). Taking dendritic cells into medicine. *Nature* **449**: 419–426.

Takakura N, Watanabe T, Suenobu S, Yamada Y, Noda T, Ito Y *et al.* (2000). A role for hematopoietic stem cells in promoting angiogenesis. *Cell* **102**: 199–209.

Taniguchi M, Harada M, Kojo S, Nakayama T, Wakao H. (2003). The regulatory role of Valpha14 NKT cells in innate and acquired immune response. *Annu Rev Immunol* **21**: 483–513.

Tatemoto K, Hosoya M, Habata Y, Fujii R, Kakegawa T, Zou MX *et al.* (1998). Isolation and characterization of a novel endogenous peptide ligand for the human APJ receptor. *Biochem Biophys Res Commun* **251**: 471–476.

Willett CG, Kozin SV, Duda DG, di Tomaso E, Kozak KR, Boucher Y *et al.* (2006). Combined vascular endothelial growth factor-targeted therapy and radiotherapy for rectal cancer: theory and clinical practice. *Semin Oncol* **33**: S35–S40.

Yamada Y, Takakura N. (2006). Physiological pathway of differentiation of hematopoietic stem cell population into mural cells. *J Exp Med* **203**: 1055–1065.

Supplementary Information accompanies the paper on the Oncogene website (http://www.nature.com/onc)

nature medicine

# Endothelial PI3K-C2α, a class II PI3K, has an essential role in angiogenesis and vascular barrier function

Kazuaki Yoshioka[1,13], Kotaro Yoshida[1,2,13], Hong Cui[1], Tomohiko Wakayama[3], Noriko Takuwa[1,4], Yasuo Okamoto[1], Wa Du[1], Xun Qi[1], Ken Asanuma[5], Kazushi Sugihara[6], Sho Aki[1], Hidekazu Miyazawa[1], Kuntal Biswas[1], Chisa Nagakura[1], Masaya Ueno[7], Shoichi Iseki[3], Robert J Schwartz[8], Hiroshi Okamoto[9], Takehiko Sasaki[5,10], Osamu Matsui[2], Masahide Asano[6], Ralf H Adams[11,12], Nobuyuki Takakura[7] & Yoh Takuwa[1]

**The class II α-isoform of phosphatidylinositol 3-kinase (PI3K-C2α) is localized in endosomes, the *trans*-Golgi network and clathrin-coated vesicles; however, its functional role is not well understood. Global or endothelial-cell–specific deficiency of PI3K-C2α resulted in embryonic lethality caused by defects in sprouting angiogenesis and vascular maturation. PI3K-C2α knockdown in endothelial cells resulted in a decrease in the number of PI3-phosphate–enriched endosomes, impaired endosomal trafficking, defective delivery of VE-cadherin to endothelial cell junctions and defective junction assembly. PI3K-C2α knockdown also impaired endothelial cell signaling, including vascular endothelial growth factor receptor internalization and endosomal RhoA activation. Together, the effects of PI3K-C2α knockdown led to defective endothelial cell migration, proliferation, tube formation and barrier integrity. Endothelial PI3K-C2α deficiency *in vivo* suppressed postischemic and tumor angiogenesis and diminished vascular barrier function with a greatly augmented susceptibility to anaphylaxis and a higher incidence of dissecting aortic aneurysm formation in response to angiotensin II infusion. Thus, PI3K-C2α has a crucial role in vascular formation and barrier integrity and represents a new therapeutic target for vascular disease.**



Formation of the vascular network by vasculogenesis and angiogenesis is essential for embryonic development, repair and remodeling of tissues in adults, and tumor growth. The angiogenic response to vascular endothelial growth factor (VEGF) and other factors begins with vascular leakage and dissolution of the subendothelial basement membrane, which is followed by the proliferation and migration of vascular endothelial cells[1,2]. Then, formation of intercellular junctions results in initial sprout formation from existing vessels. The newly formed endothelial tubes mature and become stabilized through their association with mural cells (smooth muscle cells (SMC) and pericytes)[3]. The tightness of the intercellular junctions, particularly adherens junctions composed of VE-cadherin and the associated proteins, controls vascular permeability[4,5]. Quiescent, stabilized vasculature with intact barrier integrity dominates in the healthy condition. In contrast, in pathological conditions such as tumors, the vasculature is immature and leaky. In the case of vascular insult such as that induced by excessive angiotensin II (Ang II) stimulation, increased vascular permeability is associated with leukocyte infiltration in the vascular wall and vascular disruption[6,7]. Therefore, stabilization of the vasculature and maintenance of vascular integrity is essential for vascular and tissue homeostasis[8,9].

PI3Ks comprise a family of enzymes that phosphorylate membrane inositol lipids at the 3′ position of the inositol ring. The lipid products of PI3Ks serve as important intracellular messengers by interacting with effector proteins, including protein kinases, guanine nucleotide exchangers for G proteins and actin cytoskeleton-regulating proteins. Through these actions, PI3Ks regulate a diverse array of cellular processes[10–12]. Three classes of PI3Ks exist. Class I PI3Ks, which are activated by tyrosine kinases and G protein–coupled receptors, consist of four catalytic subunits, p110α, p110β, p110γ and p110δ, and produce mainly phosphatidylinositol 3,4,5-trisphosphates (PtdIns(3,4,5)$P_3$). In endothelial cells, class I PI3Ks, in particular p110α, are indispensable for angiogenesis in the early embryo by regulating endothelial cell proliferation, migration and morphogenesis[13,14]. There is only one class III PI3K, Vps34, which generates PtdIns(3)P to regulate vesicular trafficking and autophagy[15]. In contrast to class I and III PI3Ks, the physiological functions of class II PI3Ks are not well understood. There are three members of the class II PI3K subfamily, which produce mainly PtdIns(3)P *in vivo*[16,17]: PI3K-C2α (C2α), PI3K-C2β (C2β) and PI3K-C2γ (C2γ). C2α is distinct from C2β, C2γ and other PI3K isoforms in that it has unique structural features, including a

[1]Department of Physiology, Kanazawa University School of Medicine, Kanazawa, Japan. [2]Department of Radiology, Kanazawa University School of Medicine, Kanazawa, Japan. [3]Department of Histology and Embryology, Kanazawa University School of Medicine, Kanazawa, Japan. [4]Department of Health and Medical Sciences, Ishikawa Prefectural Nursing University, Kahoku, Japan. [5]Department of Medical Biology, Akita University Graduate School of Medicine, Akita, Japan. [6]Division of Transgenic Animal Science, Advanced Science Research Center, Kanazawa University, Kanazawa, Japan. [7]Department of Signal Transduction, Research Institute for Microbial Diseases, Osaka University, Osaka, Japan. [8]Department of Biology and Biochemistry, University of Houston, Houston, Texas, USA. [9]Department of Medical Biochemistry, Tohoku University School of Medicine, Sendai, Japan. [10]Research Center for Biosignal, Akita University, Akita, Japan. [11]Max Planck Institute for Molecular Biomedicine, Department of Tissue Morphogenesis, Muenster, Germany. [12]University of Muenster, Faculty of Medicine, Muenster, Germany. [13]These authors contributed equally to this work. Correspondence should be addressed to Y.T. (ytakuwa@med.kanazawa-u.ac.jp).

Received 19 April; accepted 10 August; published online 16 September 2012; doi:10.1038/nm.2928

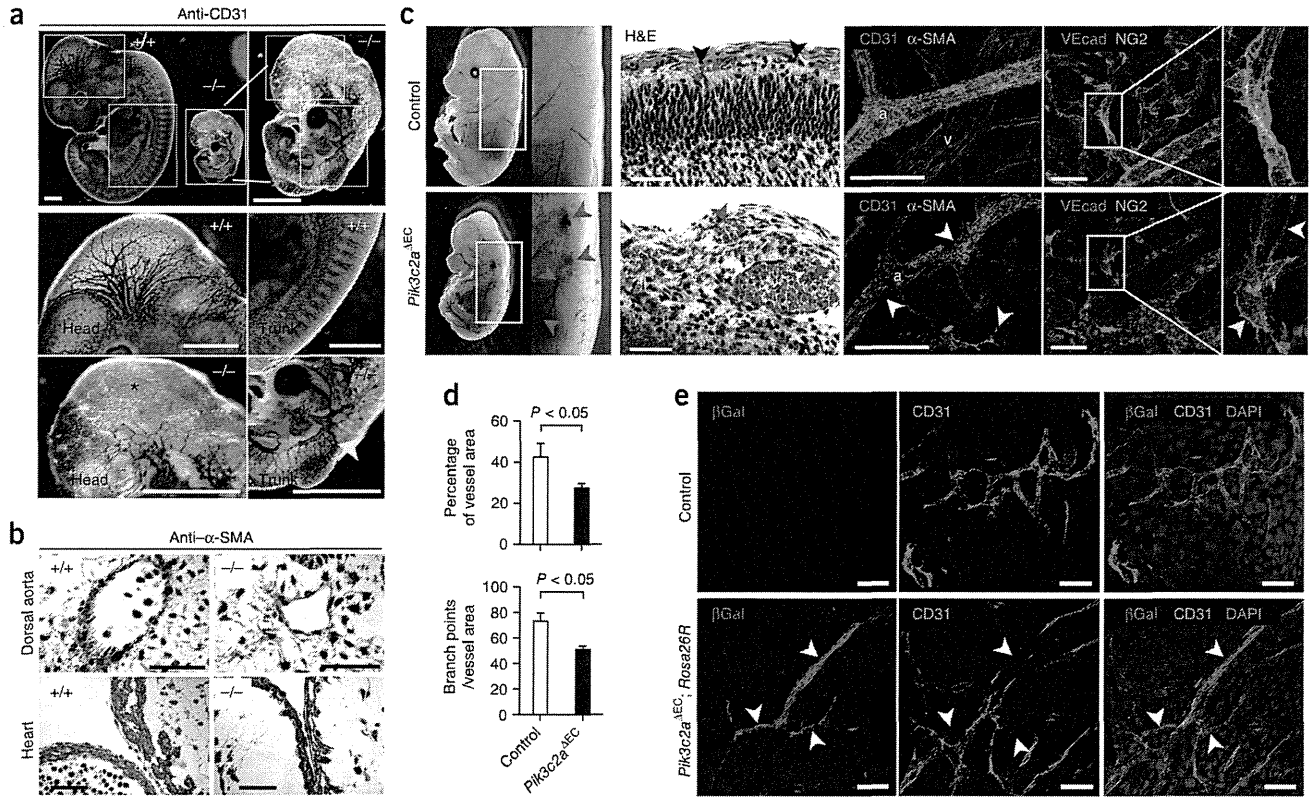


**Figure 1** Endothelial C2α is necessary for developmental angiogenesis. (**a**) Whole-mount CD31-specific immunohistochemical staining of the vasculature in E11.5 wild-type (+/+) and global *Pik3c2a*$^{-/-}$ embryos. The magnified views show the brain (asterisk, bottom left), dorsal aorta (red arrowhead, bottom right) and intersomitic vessels (yellow arrowhead, bottom right) in *Pik3c2a*$^{-/-}$ embryos. Scale bars, 2 mm. (**b**) α-SMA–specific immunohistochemical staining in cross sections of dorsal aorta and heart from E11.5 wild-type and *Pik3c2a*$^{-/-}$ embryos. Scale bars, 100 μm. (**c**) Left and middle, gross views and H&E staining of skin sections of E15.5 wild-type and homozygous endothelial-cell–specific C2α-deletion mutant (*Pik3c2a*$^{\Delta EC}$) embryos (red arrowheads, dilated vessels and hemorrhage; black arrowheads, normal dermal vessels). Right, whole-mount double immunofluorescence staining of skin sections from E15.5 control and *Pik3c2a*$^{\Delta EC}$ embryos using CD31-specific (red) and α-SMA–specific (green), and VE-cadherin–specific (VEcad, red) and NG2-specific (green) staining. For CD31 and α-SMA staining, white and yellow arrowheads indicate SMC-uncovered areas and dettached SMCs, respectively; for VE-cadherin and NG2 staining, yellow and white arrowheads indicate loosely attached and detached pericytes, respectively. a, arteriole; v, venule. Scale bars, 100 μm. (**d**) Quantification of the CD31-positive vessel area per microscopic field (%) and branch points per vessel area in the skin. $n = 6$ mice per group. Data shown are the means ± s.e.m., and statistical significance was analyzed by Mann-Whitney *U* test. (**e**) CD31-specific and β-galactosidase (βGal)-specific double immunofluorescent staining of brain sections from E15.5 control (*Pik3c2a*$^{flox/flox}$; *Rosa26R*) and endothelial-cell–specific C2α-deleted (*Pik3c2a*$^{\Delta EC}$; *Rosa26R*) embryos. White arrowheads indicate βGal-positive, CD31-negative cord-like cell clusters, which were interspersed within capillaries. Scale bars, 50 μm.



clathrin-binding site in the N-terminal stretch, and relative resistance to PI3K inhibitors[16,18]. C2α is expressed in a limited number of cell types, including the epithelium, vascular endothelium and smooth muscle[19,20]. C2α localizes to clathrin-coated endocytic vesicles, other endosomes and the *trans*-Golgi network (TGN) and has been suggested to regulate intracellular vesicular trafficking[16,18,21,22]. Previous *in vitro* studies[21,23,24] showed that various extracellular stimuli, including cytokines, insulin and integrin ligation, modestly stimulate C2α activity. However, the *in vivo* function of C2α is largely unknown, although a recent study[25] showed that a hypomorphic C2α mutant allele resulted in impairment of renal glomerular formation.

Using a gene-targeting strategy, we explored the *in vivo* role of C2α. We found that C2α has a crucial role in developmental and pathological angiogenesis in an endothelial-cell–autonomous manner. Notably, the mechanisms underlying the proangiogenic effects of C2α differ from those of class I PI3Ks: C2α regulates primarily vesicular trafficking, which is essential for normal delivery of membrane proteins, including VE-cadherin, as well as for specific aspects of cellular signaling. C2α thus has a pivotal role in endothelial cell proliferation, survival, migration, morphogenesis and, thereby, angiogenesis. A second crucial role of C2α in the vasculature is maintenance of endothelial barrier function and vascular integrity.

## RESULTS

### Endothelial C2α is crucial for physiological angiogenesis

Homozygous global C2α-deleted mutant (*Pik3c2a*$^{-/-}$) mouse embryos had retarded growth from embryonic day (E) 8.5 and died between E10.5–E11.5 as a result of defects in vascular formation (**Fig. 1**, **Supplementary Table 1** and **Supplementary Figs. 1–3**), suggesting an essential nonredundant role of class II PI3Ks in mouse development. Whole-mount CD31 staining of the embryos revealed severe defects in vascular development throughout the embryo (**Fig. 1a**). In contrast to wild-type (*Pik3c2a*$^{+/+}$) embryos, the major vessels, including the dorsal aorta, intersomitic vessels and branchial arches, were severely disorganized or absent in *Pik3c2a*$^{-/-}$ embryos (**Fig. 1a**). We were barely able to detect α-smooth muscle actin (α-SMA)-positive

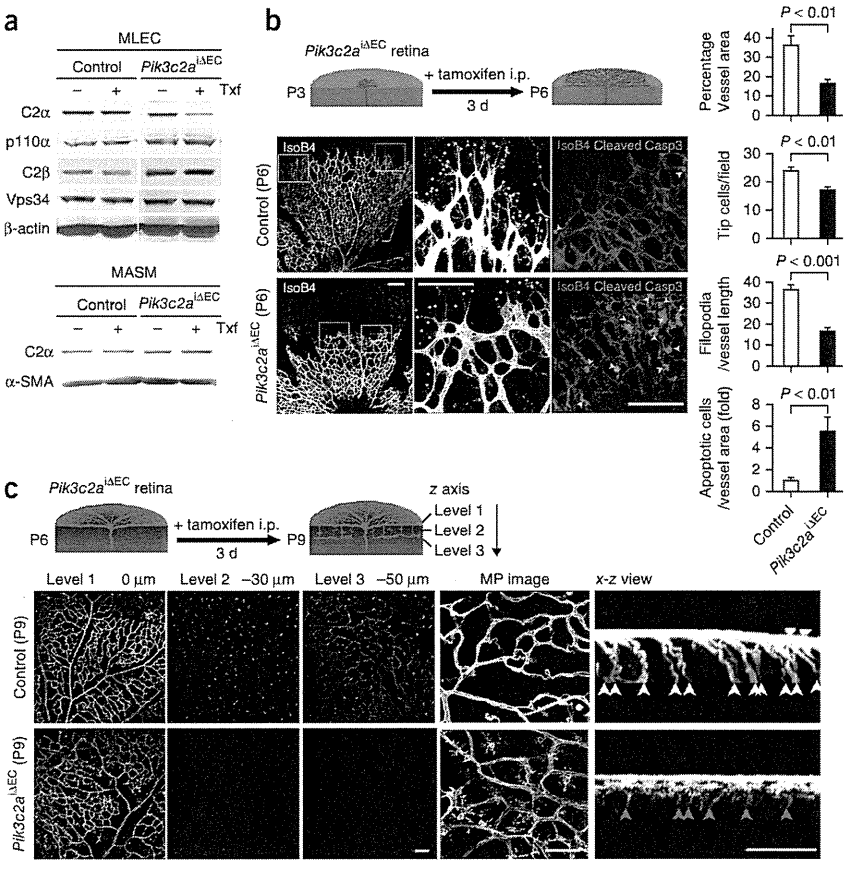


**Figure 2** C2α is required for postnatal retinal angiogenesis. (**a**) Western blot analysis of C2α, p110α, C2β and Vps34 proteins in mouse lung endothelial cells (MLEC) and aortic smooth muscle cells (MASM) from 4-week-old control (*Pik3c2a*$^{flox/flox}$) and *Pik3c2a*$^{i\Delta EC}$ mice with or without administration of tamoxifen (Txf). β-actin and α-SMA were used as loading controls. (**b**) Top, schematic of the experimental strategy to assess early formation of the retinal vasculature (P3–P6) in *Pik3c2a*$^{i\Delta EC}$ mice. Bottom, flat-mount isolectin-B4 (IsoB4) staining of retinas from control (*Pik3c2a*$^{flox/flox}$) and tamoxifen (intraperitoneally (i.p.) administered at P3)-inducible endothelial-cell–specific C2α deletion mutant (*Pik3c2a*$^{i\Delta EC}$) mice at P6. Yellow dots and arrowheads indicate filopodia and apoptotic cells, respectively. Scale bars, 100 μm. Right, quantification of vessel area per microscopic field (%) and numbers of tip cells and filopodia per microscopic field. $n = 6–11$ mice per group. Casp3, caspase-3. Data shown are means ± s.e.m., and statistical significance was analyzed by Mann-Whitney *U* test. (**c**) Top, schematic of the experimental strategy to assess late development of the retinal vasculature (P6–P9) in *Pik3c2a*$^{i\Delta EC}$ mice. Bottom, flat-mount IsoB4 staining of retinas from control and *Pik3c2a*$^{i\Delta EC}$ mice at P9. At left, images of the sections at the indicated levels are shown. At right, maximum intensity projection (MIP) stacked confocal images and an *x-z* view of the retinal vasculature showing perpendicular sprouting (white and red arrowheads) at P9 in both groups are shown. Scale bars, 50 μm.

mural cells in the *Pik3c2a*$^{-/-}$ dorsal aorta, but could readily detect such cells in the hearts of *Pik3c2a*$^{-/-}$ and wild-type embryos (**Fig. 1b**). In support of the above data, at midgestation, C2α was highly expressed in vascular endothelial cells, as well as in other cell types, including SMC, cardiomyocytes and gastrointestinal epithelium of wild-type embryos (**Supplementary Fig. 4**).

To determine in which cell type(s) C2α is required, we generated three cardiovascular-specific C2α deletion strains (**Supplementary Fig. 5**). Both SMC-specific (*Pik3c2a*$^{flox/flox}$; *SM22a*-Cre, called here *Pik3c2a*$^{\Delta SMC}$) and cardiomyocyte-specific (*Pik3c2a*$^{flox/flox}$; *Nkx2-5*-Cre (ref. 26), called here *Pik3c2a*$^{\Delta CM}$) C2α-deletion mutants developed normally and the mutant animals were born at the expected Mendelian ratio (**Supplementary Tables 2** and **3**). However, the endothelial-cell–specific C2α-deletion mutant (*Pik3c2a*$^{flox/flox}$; *Tie2*-Cre (ref. 27), called here *Pik3c2a*$^{\Delta EC}$) has an embryonic-lethal phenotype (**Supplementary Tables 3–7**) involving abnormalities in multiple organs, including severely impaired vascular formation, indicating that endothelial C2α is essential for normal vascular formation and development. The most severely affected *Pik3c2a*$^{\Delta EC}$ mutants died at E12.5 and phenocopied a global *Pik3c2a*-null embryo. *Pik3c2a*$^{\Delta EC}$ embryos also had marked dilation of subcutaneous microvessels and hemorrhage (**Fig. 1c**). Double immunofluorescent staining of *Pik3c2a*$^{\Delta EC}$ embryo tissue using CD31- and α-SMA–specific antibodies showed reductions in vascular branching and in the area covered by endothelial cells (reduced by 31% and 36%, respectively, compared with control embryos; $P < 0.05$; **Fig. 1c,d**) and discontinuous and incomplete coverage of microvessels with SMC (**Fig. 1c** and **Supplementary Fig. 6a,b**). Immunostaining using VE-cadherin–specific and neuron-glial antigen 2 (NG2)-specific antibodies revealed that capillaries had discontinuous adherens-junction formation and poor coverage with NG2-positive pericytes, which were frequently rounded and had cellular processes that were detached from the capillary wall (**Fig. 1c** and **Supplementary Fig. 6c**). In *Pik3c2a*$^{\Delta EC}$; *Rosa26R* embryos, β-galactosidase–positive, CD31-negative cord-like cell clusters were interspersed within the capillaries (**Fig. 1e**), suggesting impaired endothelial-cell differentiation in the vasculature of *Pik3c2a*$^{\Delta EC}$ embryos. Taken together, these results imply that loss of C2α expression in endothelial cells is responsible for the phenotype of *Pik3c2a*$^{-/-}$ mice.

Because *Pik3c2a*$^{\Delta EC}$ mice are embryonic lethal, we created tamoxifen-inducible, conditional endothelial-cell–specific C2α-deletion mice (*Pik3c2a*$^{i\Delta EC}$) that expressed tamoxifen-activated Cre recombinase under the control of the VE-cadherin promoter[28] (*Pik3c2a*$^{flox/flox}$; *Cdh5*(PAC)-CreER$^{T2}$; **Supplementary Fig. 5e**). We studied the role of C2α in postnatal physiological angiogenesis in these mice using a retinal angiogenesis model. Administration of tamoxifen to these mice at postnatal day (P) 3 resulted in a marked reduction in C2α protein expression at P6 in endothelial cells isolated from the lungs but not in aortic SMC (**Fig. 2a**). At P6, endothelial-cell–specific C2α inactivation induced by tamoxifen administration markedly inhibited retinal angiogenesis: vessel area, the number of tip cells and the number of filopodia at the vascularizing front were reduced by 46%, 32% and 48%, respectively, in the superficial layer of retinas from *Pik3c2a*$^{i\Delta EC}$ mice compared with those from tamoxifen-administered *Pik3c2a*$^{flox/flox}$ control mice (**Fig. 2b** and **Supplementary Fig. 7**). Perpendicular vascular sprouting and horizontal vascular network formation in the deeper retina were also severely impaired in *Pik3c2a*$^{i\Delta EC}$ retinas (**Fig. 2c**). In addition, retinas of *Pik3c2a*$^{\Delta EC}$

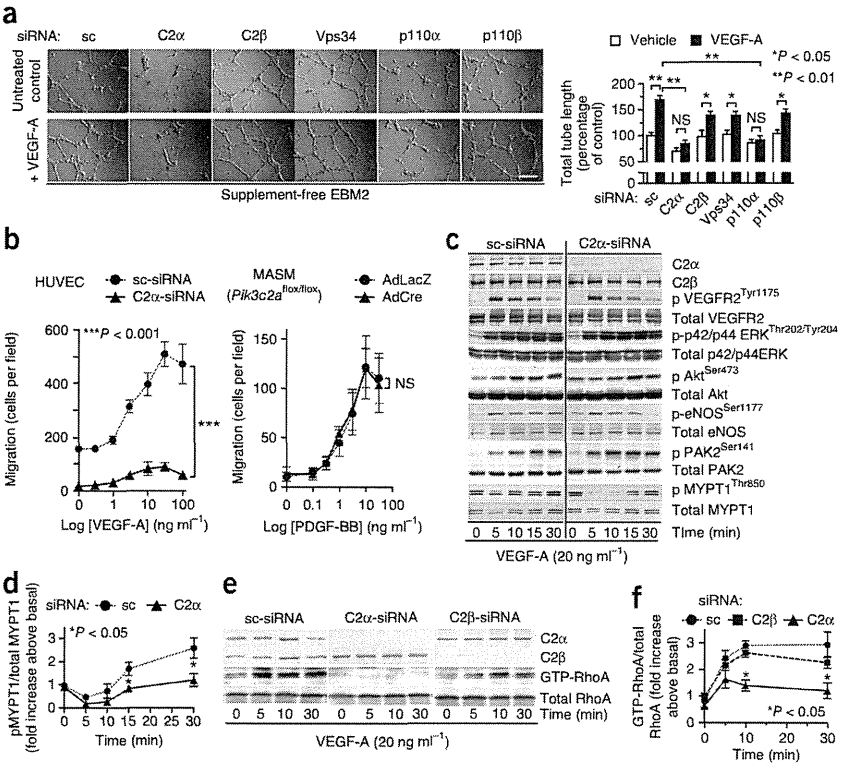


**Figure 3** Tube formation, cell migration and RhoA activation are impaired in C2α-depleted HUVEC. (**a**) Effects of siRNA-mediated PI3K knockdown on VEGF-A (20 ng ml$^{-1}$)-induced tube formation in serum-free and growth factor supplement–free medium. Scale bar, 200 μm. Quantification of total tube length (right). NS, not significant; sc, scrambled siRNA control. (**b**) Effects of C2α knockdown or deletion on VEGF-A–directed HUVEC migration and PDGF-BB–directed MASM migration. AdLacZ, adenovirus expressing β-galactosidase; AdCre, adenovirus expressing Cre. Data are means ± s.e.m. (**c**) Western blot analysis of the indicated proteins after treatment of control or C2α-depleted HUVEC following VEGF-A (20 ng ml$^{-1}$) treatment at the indicated time points. (**d**) Quantification of VEGF-A–induced phosphorylation of MYPT1. (**e**) Western blot analysis of the indicated proteins after treatment of control or C2α- or C2β-depleted HUVEC following VEGF-A (20 ng ml$^{-1}$) treatment at the indicated time points. (**f**) Quantification of the results in **e**. Data in **d** and **f** are shown as relative values of the normalized band intensities. For **a**, **b**, **d** and **f**, data shown are means ± s.e.m. of three independent experiments. Statistical significance was analyzed by two-way analysis of variance (ANOVA).



mice showed a marked (5.5-fold) increase in apoptosis compared to those of control littermates ($P < 0.01$; **Fig. 2b**). Mice with hemizygous *Pik3c2a* endothelial-cell–specific deletion (*Pik3c2a*$^{flox/+}$; *Tie2*-Cre mice) also showed decreased retinal angiogenesis with reduced numbers of tip cells and filopodia at the vascularizing front as well as reduced endothelial cell proliferation (**Supplementary Fig. 8**).

### C2α is involved in endothelial cell function through RhoA

In human umbilical vein endothelial cells (HUVEC) cultured in serum and growth factor supplement–free medium, knockdown of either p110α or C2α by specific siRNAs, but not knockdown of other PI3Ks by C2β-, Vps34- or p110β-specific siRNAs, inhibited VEGF-A–induced capillary-like tube formation (**Fig. 3a** and **Supplementary Fig. 9a,b**). In HUVEC cultured in complete growth medium with serum and growth-factor supplements (endothelial basal medium 2 (EBM2)), knockdown of C2α inhibited tube formation, whereas knockdown of p110α or other PI3Ks did not have this effect; knockdown of p110α and p110β together inhibited tube formation of cells cultured in EBM2 (**Supplementary Fig. 9c**).

C2α knockdown also markedly inhibited transwell migration of HUVEC toward VEGF-A ($P < 0.001$; **Fig. 3b**) but not migration of SMC toward platelet-derived growth factor BB (PDGF-BB), augmented HUVEC apoptosis (**Supplementary Fig. 9d,e**) and modestly inhibited HUVEC serum-induced proliferation (**Supplementary Fig. 9f**). In contrast, Cre-mediated deletion of C2α had no effect on SMC proliferation (**Supplementary Fig. 9g**). These results indicate specific, essential roles for C2α in endothelial cell activities.

C2α silencing did not alter VEGF-A–induced phosphorylation of VEGF receptor 2 (VEGFR2), p42/p44 extracellular signal-regulated kinase (ERK), Akt, endothelial nitric oxide synthase (eNOS) or p21-activated kinase-2 (PAK2) (**Fig. 3c**), which is in contrast to the effects of p110α knockdown[10–13]. However, C2α knockdown markedly inhibited VEGF-A–induced phosphorylation of myosin phosphatase target subunit 1 (MYPT1), a substrate of Rho kinase (**Fig. 3c,d**), and activation of the small GTPase RhoA (**Fig. 3e,f**). Consistent with these results, immunostaining using an antibody that specifically recognizes the GTP-bound active form of RhoA (**Supplementary Fig. 10a**) showed that knockdown of either C2α or p110α suppressed VEGF-A–induced RhoA activation (**Supplementary Fig. 10b**). Knockdown of C2α but not p110α or Vps34 also inhibited serum and growth factor-induced activation of RhoA (**Supplementary Fig. 10c**). In addition, C2α knockdown reduced activation of two other small GTPases: Rac1 activation induced by VEGF-A and Rap1 activation induced by fibroblast growth factor 2 (FGF2) (**Supplementary Fig. 11**). Both Rac1 and Rap1 as well as RhoA help stabilize VE-cadherin at contacts between endothelial cells[5,29].

RhoA knockdown, as well as VE-cadherin knockdown, abolished VEGF-A–induced tube formation ($P < 0.01$; **Supplementary Fig. 12a,b**). In a mixed culture of HUVEC, in which cells expressing the dominant-negative RhoA mutant RhoA$^{Asn19}$ were mixed with LacZ-transfected control cells, RhoA$^{Asn19}$-expressing HUVEC were rounded and did not form cell-cell contacts through cell protrusions as did control HUVEC (**Supplementary Fig. 12c,d**). Together, these observations suggest that C2α has an essential role in endothelial morphogenesis through mechanisms involving RhoA.

### C2α is required for endosomal trafficking of VE-cadherin

To study effects of C2α on endosomal trafficking, we first transfected HUVEC with the PtdIns(3)P-specific probe monomeric red fluorescent protein (mRFP)-tagged 2 × FYVE domain[30,31]. In control HUVEC treated with scrambled (sc) siRNA, the mRFP-2 × FYVE signal was localized mainly to endosomes (**Fig. 4a**). Depletion of C2α, but not of p110α or Vps34, markedly reduced the number of mRFP-2 × FYVE$^{+}$ vesicles ($P < 0.01$). The total cellular content of PtdIns(3)P, but not of PtdIns(3,4)$P_2$, PtdIns(3,5)$P_2$ or PtdIns(3,4,5)$P_3$,

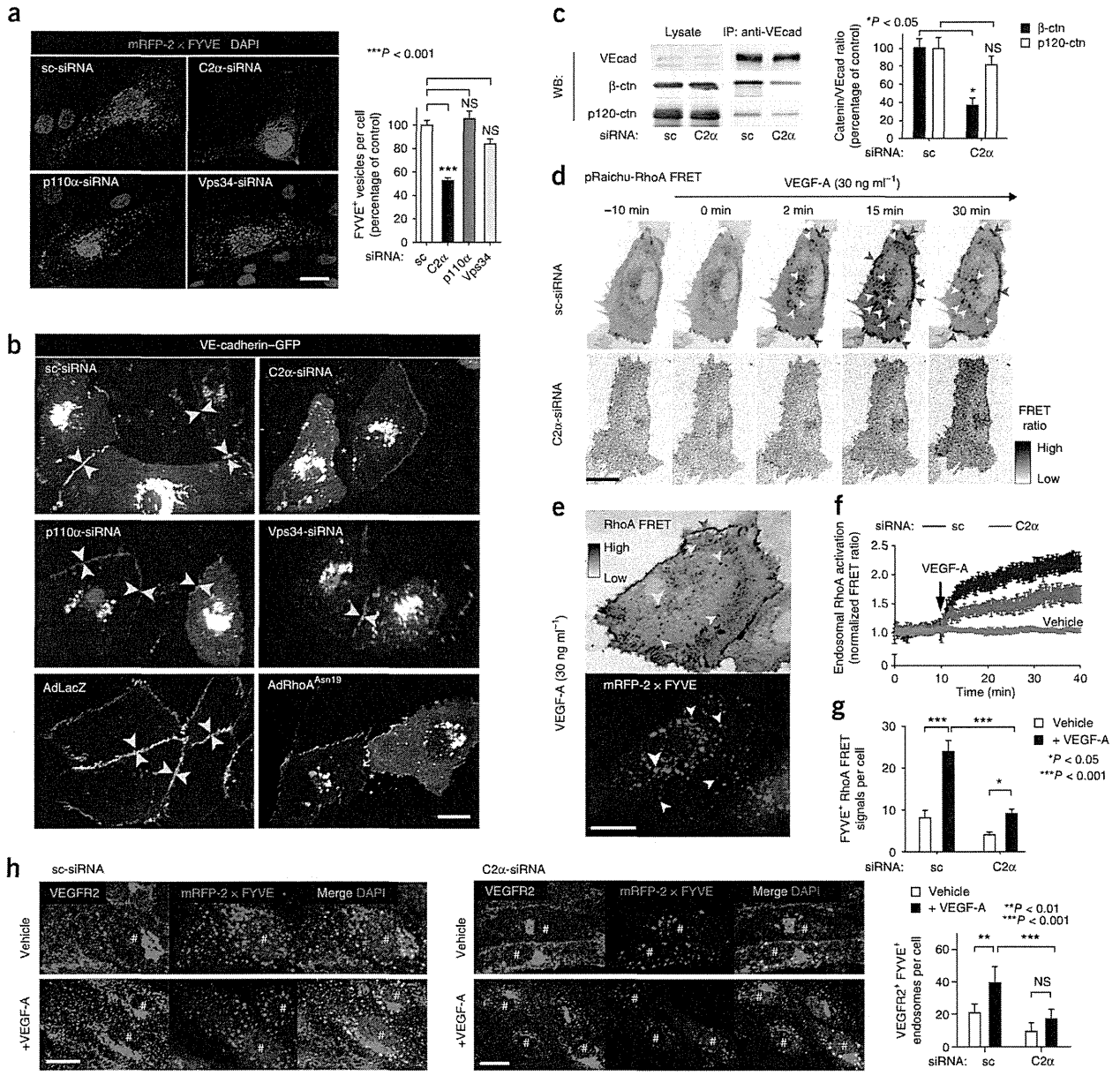


**Figure 4** Endosomal transport, VE-cadherin assembly at cell junctions and the activation of endosomal RhoA are impaired in C2α-depleted endothelial cells. (**a**) Left, fluorescent imaging of sc-siRNA–treated control HUVEC and C2α-, p110α- or Vps34-depleted HUVEC transfected with the mRFP-2 × FYVE domain. Scale bar, 20 μm. Right, quantification of the number of mRFP-2 × FYVE$^+$ (FYVE$^+$) vesicles per cell. $n$ = 11–14 cells per group. NS, not significant. (**b**) Fluorescent imaging of VE-cadherin–GFP trafficking in sc-siRNA–treated control HUVEC, C2α-, p110α- or Vps34-depleted HUVEC and AdLacZ- or AdRhoA$^{Asn19}$-transfected HUVEC. Yellow arrowheads indicate VE-cadherin$^+$ cell-cell contacts. Asterisks indicate gaps between HUVEC. Scale bar, 20 μm. See also **Supplementary Videos 4** and **5**. (**c**) Immunoprecipitation (IP) and western blot (WB) analyses to assess association of β-catenin (β-ctn) and p120-catenin (p120-ctn) with VE-cadherin (VEcad). VE-cadherin was immunoprecipitated from HUVEC treated with the indicated siRNAs, followed by western blotting for the indicated proteins. Western blots of the cell lysate without immunoprecipitiation are shown as a control. Quantification of the results is shown at right. Data from three independent experiments are shown. (**d–g**) HUVEC transfected with the FRET probe expression vector pRaichu-RhoA were used to assess RhoA activation. (**d**) At the indicated time points after treatment with VEGF-A, RhoA activation was visualized on endosomes (yellow arrowheads) and on plasma membrane at cell-cell contacts (red arrowheads) in control (sc-siRNA) and C2α-depleted HUVEC. (**e**) VEGF-A–induced RhoA activation in HUVEC cotransfected with pRaichu-RhoA and mRFP-2 × FYVE. Colocalization was observed between FRET signals (yellow arrowheads, top) and mRFP-2 × FYVE$^+$ endosomes (white arrowheads, bottom). Red arrowheads (top) indicate RhoA activation at cell-cell contacts. Scale bar, 20 μm. (**f**) Quantification of endosomal RhoA activation in control and C2α-depleted HUVEC at the indicated time ponts after VEGF or vehicle (M199 medium) addition. $n \geq 8$ cells per group. (**g**) Quantification of mRFP-2 × FYVE$^+$ FRET signals in HUVEC 15 min after VEGF-A or vehicle addition. $n$ = 9–22 cells per group. (**h**) Immunofluorescence staining of VEGFR2 (green) and mRFP-2 × FYVE staining in cells cotransfected with the mRFP-2 × FYVE construct and either sc-siRNA or C2α-targeting siRNA. The cells were treated with VEGF-A or vehicle as indicated. Quantification of the number of VEGFR2$^+$ FYVE$^+$ endosomes per cell is shown at right. #, mRFP-2 × FYVE–transfected cells. $n$ = 8–20 cells per group. Scale bars, 20 μm. In **a**, **c**, **g** and **h**, data shown are means ± s.e.m. Statistical significance was analyzed by one-way ANOVA for **a** and two-way ANOVA for **c**, **g** and **h**.

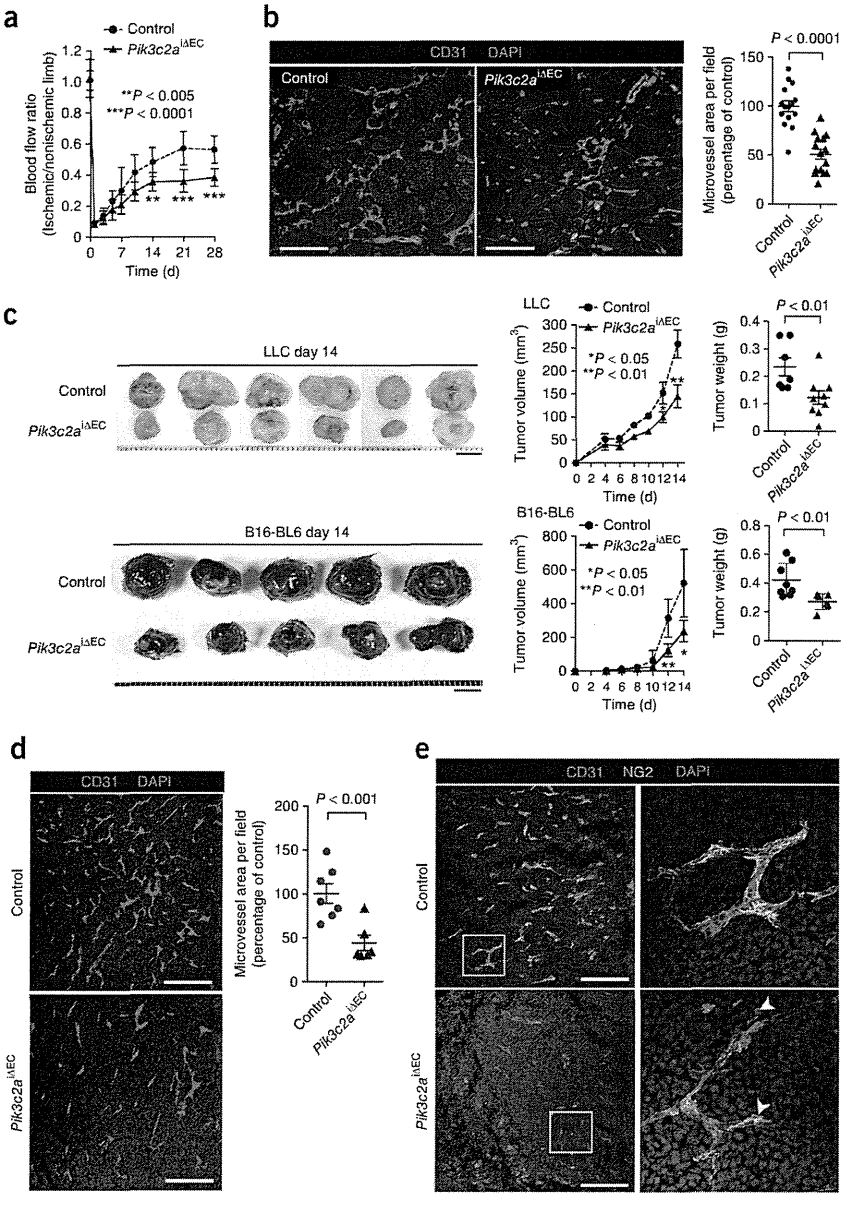


**Figure 5** Targeted deletion of endothelial C2α reduces postischemic and tumor angiogenesis. (**a**,**b**) Postischemic hindlimb angiogenesis. (**a**) The ratio of ischemic to nonischemic limb laser Doppler blood flow in male 8-week-old control (*Pik3c2a*$^{flox/flox}$) and homozygous endothelial-cell–specific C2α deletion mutant (*Pik3c2a*$^{i\Delta EC}$) mice at the indicated time points following ischemic injury. $n = 13$ mice per group. Data shown are means ± s.e.m. Statistical significance was analyzed by two-way ANOVA. (**b**) CD31-specific immunofluorescence staining of sections of ischemic hindlimb muscle in control and *Pik3c2a*$^{i\Delta EC}$ mice. Nuclei (blue) were stained with DAPI. Scale bars, 100 μm. Quantification of CD31$^+$ microvessel density on day 28 after injury is shown at right. $n \geq 20$ fields from at least eight mice. Statistical significance was analyzed by Mann-Whitney *U* test. (**c**) Representative LLC (top) and B16-BL6 tumors (bottom) in male 10-week-old control and *Pik3c2a*$^{i\Delta EC}$ mice. Scale bars, 5 mm. Quantification of tumor volume and weight (day 14) is shown at right. $n \geq 7$ mice per group. Data shown are means ± s.e.m. (**d**) CD31-specific immunofluorescence staining of LLC tumor sections in control and *Pik3c2a*$^{i\Delta EC}$ mice. Scale bars, 200 μm. Quantification of CD31$^+$ microvessel density is shown at right. $n = 7$ mice per group. Statistical significance was analyzed by two-way ANOVA for tumor volumes and by Mann-Whitney *U* test for tumor weights. (**e**) CD31- and NG2-specific double immunofluorescence staining of LLC tumor sections in control and *Pik3c2a*$^{i\Delta EC}$ mice. Yellow and white arrowheads indicate loose attachment and detachment of pericytes, respectively, in *Pik3c2a*$^{i\Delta EC}$ mice. Scale bars, 200 μm. Nuclei (blue) were stained with DAPI.



was reduced in C2α-depleted cells compared to control cells (**Supplementary Fig. 13**). Thus, C2α is needed for normal PtdIns(3)P accumulation in the endosomal compartment. Consistent with this idea, we detected C2α in a granular pattern in HUVEC, with enrichment in the perinuclear region, and found that C2α partially colocalized with markers of clathrin-coated vesicles, the TGN and early endosomes (**Supplementary Fig. 14a–c**)[16,18,22]. The intracellular localization of GFP-C2α also substantially overlapped with that of mRFP-2 × FYVE (**Supplementary Fig. 15a** and **Supplementary Video 1**). The motility, fusion and fission of GFP-tagged 2 × FYVE$^+$ vesicles were markedly attenuated in C2α-depleted cells (**Supplementary Videos 2** and **3**), suggesting that C2α is involved in endosomal trafficking. Knockdown of C2α, but not of p110α or Vps34, caused enlargement of the Golgi and TGN area (**Supplementary Fig. 14d**). We also found swelling of the Golgi and TGN compartment in endothelial cells of dorsal aortas from *Pik3c2a*$^{-/-}$ mice, as assessed by electron microscopy (**Supplementary Fig. 14e**).

In C2α-depleted but not p110α- or Vps34-depleted HUVEC, the trafficking of VE-cadherin between the TGN and intercellular junctions at the plasma membrane was disrupted (**Fig. 4b** and **Supplementary Videos 4** and **5**). C2α was partially colocalized with VE-cadherin in the Golgi and TGN area and in endosomes but this colocalization was not evident at intercellular junctions (**Supplementary Fig. 15b**). A portion of the mRFP-2 × FYVE$^+$ vesicles were positive for VE-cadherin–GFP, suggesting transport of VE-cadherin by PtdIns(3)P$^+$ vesicles (**Supplementary Fig. 15c**). In agreement with these findings, the accumulation of VE-cadherin at cell-cell contacts in C2α-depleted but not p110α- or Vps34-depleted HUVEC was reduced and the staining for VE-cadherin was discontinuous (**Supplementary Fig. 16b**). C2α-depleted cells also showed a reduced association of VE-cadherin with β-catenin as well as instability of VE-cadherin protein (**Fig. 4c** and **Supplementary Fig. 16a**). Expression of RhoA$^{Asn19}$ in HUVEC impaired VE-cadherin trafficking between the TGN and the plasma membrane, resulting in disturbed VE-cadherin clustering at cell-cell contacts (**Fig. 4b**, **Supplementary Video 6** and **Supplementary Fig. 16c**). In mixed cultures of normal and RhoA-depleted HUVEC, VE-cadherin clustering was impaired at the boundaries between RhoA-depleted cells (**Supplementary Fig. 16d**). In C2α-depleted HUVEC, expression

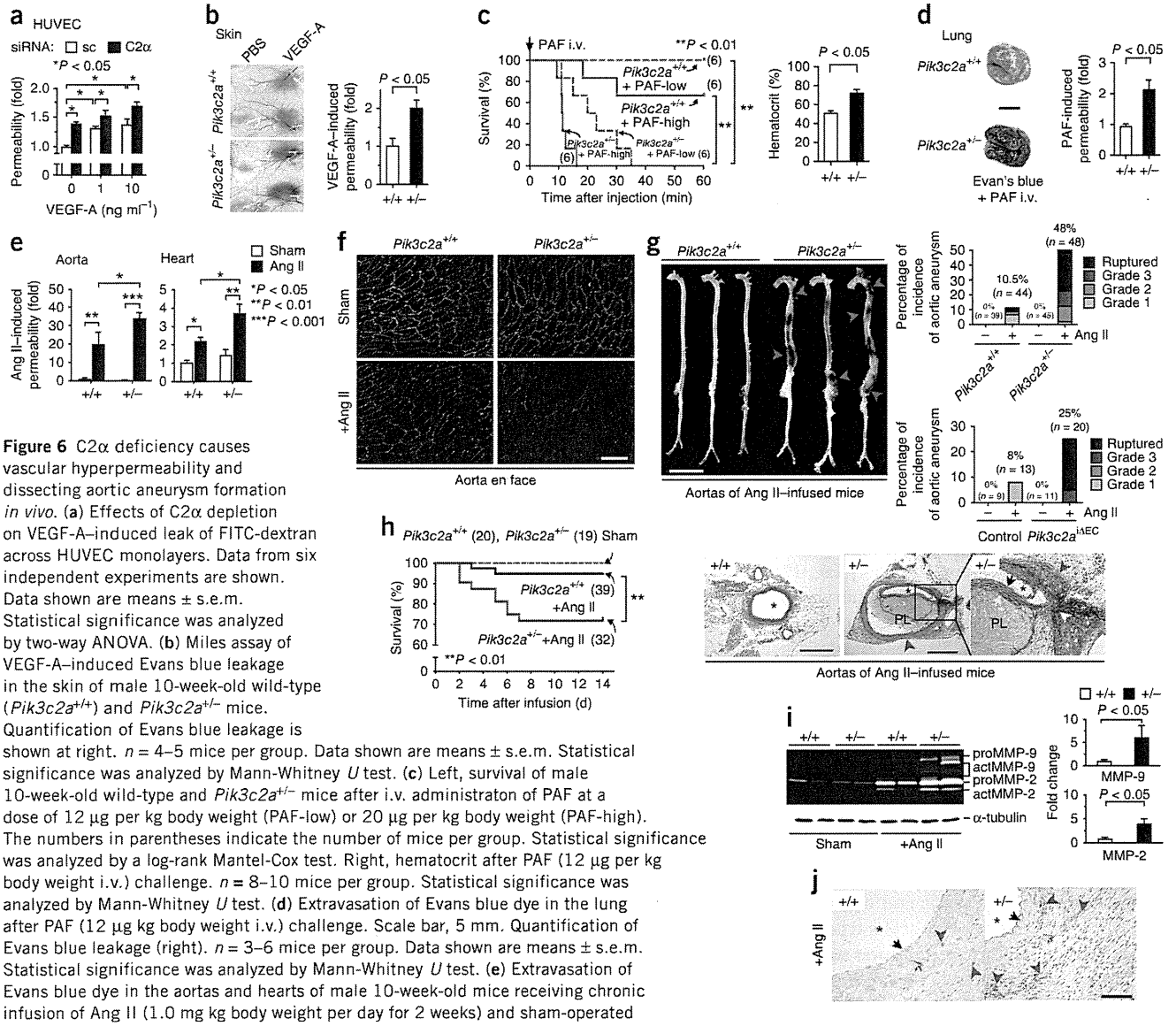


**Figure 6** C2α deficiency causes vascular hyperpermeability and dissecting aortic aneurysm formation *in vivo*. (**a**) Effects of C2α depletion on VEGF-A–induced leak of FITC-dextran across HUVEC monolayers. Data from six independent experiments are shown. Data shown are means ± s.e.m. Statistical significance was analyzed by two-way ANOVA. (**b**) Miles assay of VEGF-A–induced Evans blue leakage in the skin of male 10-week-old wild-type (*Pik3c2a*$^{+/+}$) and *Pik3c2a*$^{+/-}$ mice. Quantification of Evans blue leakage is shown at right. $n = 4$–5 mice per group. Data shown are means ± s.e.m. Statistical significance was analyzed by Mann-Whitney *U* test. (**c**) Left, survival of male 10-week-old wild-type and *Pik3c2a*$^{+/-}$ mice after i.v. administraton of PAF at a dose of 12 μg per kg body weight (PAF-low) or 20 μg per kg body weight (PAF-high). The numbers in parentheses indicate the number of mice per group. Statistical significance was analyzed by a log-rank Mantel-Cox test. Right, hematocrit after PAF (12 μg per kg body weight i.v.) challenge. $n = 8$–10 mice per group. Statistical significance was analyzed by Mann-Whitney *U* test. (**d**) Extravasation of Evans blue dye in the lung after PAF (12 μg kg body weight i.v.) challenge. Scale bar, 5 mm. Quantification of Evans blue leakage (right). $n = 3$–6 mice per group. Data shown are means ± s.e.m. Statistical significance was analyzed by Mann-Whitney *U* test. (**e**) Extravasation of Evans blue dye in the aortas and hearts of male 10-week-old mice receiving chronic infusion of Ang II (1.0 mg kg body weight per day for 2 weeks) and sham-operated control mice. $n = 3$–5 mice per group. Data shown are means ± s.e.m. Statistical significance was analyzed by two-way ANOVA. (**f**) En face confocal microscopic views of VE-cadherin–specific immunofluorescent staining of aortas from male 10-week-old mice treated with Ang II. Scale bar, 50 μm. (**g**) Aneurysm formation in *Pik3c2a*$^{+/+}$ and *Pik3c2a*$^{+/-}$ mice treated with Ang II. Top left, gross view of aortic aneurysms (red arrowheads, top left). Scale bar, 1 mm. Top right, incidence and severity of aortic aneurysms in AngII-treated and nontreated, sham-operated *Pik3c2a*$^{+/-}$ and *Pik3c2a*$^{i\Delta EC}$ mice. See the Online Methods for how aneurysm severity was graded. Bottom, azan-stained sections of dissecting aortic aneurysm in AngII-treated *Pik3c2a*$^{+/-}$ mice. Scale bars, 500 μm. PL, pseudolumen; red arrowheads, adventitia; black arrow, internal elastic lamina; yellow arrow, external elastic lamina; asterisks, true lumen of the aorta. (**h**) Survival of Ang II-treated and nontreated, sham-operated male 8- to 10-week-old *Pik3c2a*$^{+/+}$ and *Pik3c2a*$^{+/-}$ mice. The numbers in parentheses indicate the number of mice in each group. Statistical significance was analyzed by a log-rank Mantel-Cox test. (**i**) Left, MMP-2 and MMP-9 activity as assessed by zymography in the aortas of Ang II-treated and nontreated, sham-operated 10-week-old male *Pik3c2a*$^{+/+}$ and *Pik3c2a*$^{+/-}$ mice. proMMP-2 and proMMP-9, MMP-2 and MMP-9 proenzymes; actMMP-2 and actMMP-9, active MMP-2 and MMP-9. Right, quantification of MMP-2 and MMP-9 activities. The sum of the proMMP-2 and actMMP-2 band densities and the sum of the proMMP-9 and actMMP-9 band densities were defined as MMP-2 and MMP-9 total activities, respectively. $n = 6$ mice per group. Data shown are means ± s.e.m. Statistical significance was analyzed by Mann-Whitney *U* test. (**j**) Mac-3–specific immunohistochemical staining of the aortic walls of male *Pik3c2a*$^{+/+}$ and *Pik3c2a*$^{+/-}$ 10-week-old mice treated with Ang II. Red arrowheads, infiltrating macrophages; black arrows, internal elastic lamina; yellow arrows, external elastic lamina. Scale bar, 200 μm.

of a GFP-tagged constitutively active RhoA mutant, Rho$^{Val14}$, but not of GFP-tagged wild-type RhoA, partially restored defective VE-cadherin clustering at cell-cell contacts (**Supplementary Fig. 16e**). In contrast, in sc-siRNA–treated control HUVEC, expression of GFP-tagged RhoA$^{Asn19}$, but not of GFP-tagged wild-type RhoA, attenuated VE-cadherin assembly at cell junctions. Thus, RhoA is required for VE-cadherin assembly at the cell junctions of endothelial cells.

As our results indicate that C2α is necessary for endosomal trafficking, and as endosomes are now recognized as being involved in the activation of signaling molecules, including Rho GTPases[32], we next explored where C2α-dependent RhoA activation occured in cells. We visualized RhoA activation by adopting a fluorescence resonance energy transfer (FRET) imaging technique. We transfected HUVEC with an expression vector for a chimeric RhoA-FRET probe protein,